

# Eco-friendly PVA-chitosan adsorbent films for the removal of azo dye Acid Orange 7: Physical cross-linking, adsorption process, and reuse of the material



John Perez-Calderon <sup>a</sup>, Diego Alejandro Marin-Silva <sup>a</sup>, Noemi Zaritzky <sup>a, b</sup>,  
 Adriana Pinotti <sup>a, b, \*</sup>

<sup>a</sup> CIDCA (Centro de Investigación y Desarrollo en Criotecología de Alimentos) CONICET-Facultad de Ciencias Exactas Universidad Nacional de La Plata (UNLP), CIC-PBA, Calle 47 y 116, La Plata, Buenos Aires, Argentina

<sup>b</sup> Departamento de Ingeniería Química- Fac.de Ingeniería-UNLP, Argentina

## ARTICLE INFO

### Article history:

Received 12 September 2022

Received in revised form

14 November 2022

Accepted 5 December 2022

### Keywords:

Hybrid film

Biosorbent

Azo dye

Chitosan

PVA

Physical cross-linking

## ABSTRACT

The treatment of wastewater requires the use of eco-friendly and cost-efficient adsorbents. A hybrid adsorbent film based on biodegradable polymers (poly(vinyl alcohol) (PVA) and chitosan (Ch) was developed to remove Acid Orange 7 (AO7), an azo dye from the textile industry present in industrial wastewaters. The polymeric adsorbent material was submitted to a curing process with different time-temperature combinations which improved its physical stability in aqueous media. This result was supported by modulated differential scanning calorimetry (MDSC) and thermogravimetric analysis (TGA). ATR-FTIR also confirmed the electrostatic interactions by hydrogen bonds between PVA and Ch, as well as among the polymers and the dye. The best curing condition to reach a high removal without weight loss was the combination of 160°C-1h.

Dye adsorption depended mainly on pH, adsorbent dose, contact time, temperature, and coexisting anions. The maximum removal efficiency (>91%) was achieved at pH = 2.5. The adsorption kinetics followed the Lagergren pseudo first-order rate equation and the adsorption isotherm was best described by the Redlich-Peterson model. As far as the authors know, the maximum adsorption capacity ( $Q_m$ ) of the adsorbent film obtained in the present work is the highest value reported in literature ( $Q_m = 678$  mg/g at 298 K and pH = 2.5). Physisorption would be the dominant mechanism at pH 4.0 while at pH 2.5 the process was conducted by chemisorption. Regeneration studies showed that composites could be used for five consecutive cycles without losing their adsorption capacity.

Thus, the use of the developed eco-compatible biodegradable materials would allow easy regeneration without losing removal selectivity, a key feature in the development of environmentally friendly sorbent materials.

© 2022 Kingfa Scientific and Technological Co. Ltd. Publishing services by Elsevier B.V. on behalf of KeAi Communications Co. Ltd. This is an open access article under the CC BY-NC-ND license (<http://creativecommons.org/licenses/by-nc-nd/4.0/>).

## 1. Introduction

Environmental remediation involves different issues, including the treatment of contaminated industrial wastewater. The textile industry is one of the most water-intensive industries [1] which implies that a large volume of dyes and chemical waste is discharged [2].

Synthetic dyes cause a significant health threat to ecology and humans due to their high chemical and biological oxygen demands, carcinogenicity, mutagenicity, potential toxicity, and even teratogenicity [3–5]. Removal of these contaminants is a challenge since synthetic dyes exhibit high resistance to biodegradation. They not only affect aquatic life by blocking the penetration of sunlight into the water body and hindering photosynthesis but also the dyes decrease the aesthetic value of the water bodies [6,7].

Azo dyes, characterized by having a chromophore azo group ( $-N=N-$ ) and an electron receptor sulfonate group ( $-SO_3^-$ ), have participation between 50 and 65% in the industry [8,9]. More

\* Corresponding author. CIDCA- Fac. Cs. Exactas UNLP, Calle 47 y 116-La Plata, 1900, Argentina. Fax: +54 221 4254853/4249287/4890741.

E-mail address: [adriana.pinotti@ing.unlp.edu](mailto:adriana.pinotti@ing.unlp.edu) (A. Pinotti).

**Abbreviations and nomenclature**

AFA	After the first adsorption cycle	NI	Not identified
ALA	After the last adsorption cycle	NR	Not reported
ALD	After the last desorption cycle	Ps1	Pseudo-first-order
ANOVA	Analysis of variance	Ps2	Pseudo-second-order
AO7	Acid Orange 7	PVA	Poly(vinyl alcohol)
ATR-FTIR	Attenuated total reflection-Fourier transform infrared spectroscopy	Q	Adsorption capacity
BFA	Before the first adsorption cycle	$Q_e$	Adsorption capacity at equilibrium
BI	Browning index	$R^2$	Coefficient of determination
CA	Contact angle	Re%	Removal percentage
Ch	Chitosan	RH	Relative humidity
DR	Dubinin-Radushkevich model	RP	Redlich-Peterson model
DTG	First derivative of thermogravimetric analysis	SD	Standard deviation
E	Tensile stress	SEM	Scanning electron microscopy
MAPE	Mean percentage error	Sw%	Swelling degree
MDSC	Modulated differential scanning calorimetry	TGA	Thermogravimetric analysis
MSR-DK	Mixed diffusion-adsorption model	$W_L\%$	Weight loss
		$\epsilon_r\%$	Percent elongation
		$\chi^2$	Chi-square error distribution parameter

specifically, acid orange 7 (AO7) is highly toxic, and its ingestion can cause eye, skin, mucous membrane, and upper respiratory tract irritations, nausea, headaches, dizziness, and loss of bone marrow leading to anemia [10]. Bladder tumors may occur by exposure to 1-amino-2-naphthol due to the reduction of AO7 [10,11]. Also, inside the human body, AO7 can form aromatic amines which can cause methemoglobinemia. The intermediate amines favor the oxidation from the ferrous form of iron ( $Fe^{2+}$ ) to the ferric state ( $Fe^{3+}$ ) which makes the heme moiety incapable of carrying oxygen and thus resulting in some characteristic symptoms such as cyanosis of the lip and nose, dizziness, and weakness [10]. Several studies have reported the development of materials for AO7 dye removal [10,12,13].

A wide variety of technologies have been implemented to remove synthetic dyes from wastewater, such as biological treatments, coagulation/flocculation, advanced oxidation processes, filtration processes, and electrochemical techniques [2]. However, various inadequacies, such as high operational costs, inefficiency, and generation of toxic byproducts, hinder the applicability of these techniques for wastewater treatment [10].

The adsorption process is cost-effective, efficient, and easy to implement at an industrial scale and the dye removed can be recovered by regenerating the adsorbent material [8,14]. The adsorption process imparts no side effects or toxicity to the water achieving a superior removal of inorganic waste constituents as compared with the conventional treatments. This process is capable of removing the pollutant in its ionic or molecular form without breaking or converting it into another product/by-product [15].

Several studies have been carried out to develop various adsorbents, such as activated carbon [16–18], metal-organic frameworks [19], polymers [20], and zeolites [21], but the high cost and environmental toxicity of these adsorbents limit the range of their applicability. Therefore, there is an urgent need for alternative adsorbents that are environmentally friendly, inexpensive, and widely available [22]. According to Mittal et al. [15], a low-cost adsorbent must be abundant in nature, a by-product or waste material from another industry, and needs very less processing before use. In this sense, the development of adsorbent materials composed of a bio-based material and a synthetic biodegradable material could be an effective strategy to improve the mechanical resistance, controlling their water sensibility while retaining their adsorption capability.

Chitosan (poly- $\beta$ -(1 → 4)-2-amino-2-deoxy-D-glucose) is a polysaccharide obtained by N-deacetylation of chitin (poly- $\beta$ -(1 → 4)-N-acetyl-D-glucosamine) which is extracted from fishing industry waste [23]. Chitosan is a natural cationic polyelectrolyte due to the presence of amino groups ( $NH_3^+$ ) when the pH of the medium is lower than chitosan pKa ( $pKa = 6.2$ ).

Chitosan (Ch) has different attributes such as low toxicity, high biocompatibility, biodegradability, and antimicrobial properties, among others [24,25]. This biopolymer is used for the generation of materials and products in biomedical, cosmetic, nutraceutical, food industries, and environmental remediation applications [24]. In this last area, Ch is well known for the production of films/membranes as adsorbent materials for synthetic dyes removal [26,27] and other pollutants such as heavy metals [25], phosphate [28], fluoride [29], and emergent pollutants [30].

Poly(vinyl alcohol) (PVA) is a hydrophilic biocompatible biodegradable polymer formed by vinyl acetate and hydrolyzed vinyl alcohol units (hydroxyl groups available). This synthetic polymer has high thermal stability, excellent mechanical properties, and resistance to extreme pH conditions [31].

Different authors have mentioned chemical crosslinking [14,32] or blending with other polymers [33,34] as strategies to improve the performance of biosorbent materials. Similarly, Ch has been coupled with manganese ferrite biochar [35], amidoxime [36], fluoroapatite [25], and silica/hydroxyapatite [37] to demonstrate high adsorption capabilities along with improved adsorbent stabilities.

Furthermore, the PVA-Ch blend yields hybrid biocomposite films with good mechanical and chemical properties due to the formation of inter/intramolecular hydrogen bonds enhancing the polymeric network [24,38,39], foams [40], nanoelectrospun fibers [41], hydrogels [42], and films [33] are different PVA-Ch materials used as efficient biosorbents for the removal of synthetic dyes.

The use of covalent crosslinkers such as glutaraldehyde or epichlorohydrin can improve the properties related to water affinity (solubility and swelling) but the toxicity limits their usefulness in eco-friendly applications [43]. Thermal curing of PVA-Ch materials decreases the swelling and solubility of the material, improving the chemical and mechanical resistance [44].

To the best of our knowledge, there is hardly any study combining the development and application of eco-friendly materials based on PVA and Ch physically crosslinked as an adsorbent of synthetic dyes.

Herein, a hybrid film was developed by assembling PVA and Ch polymers. Then the biodegradable material was modified by a curing process and used as an adsorbent of the azo-dye AO7.

The PVA-Ch film was characterized by using attenuated total reflection-Fourier transform infrared spectroscopy (ATR-FTIR), scanning electron microscopy (SEM), thermal analysis (modulated differential scanning calorimetry and thermogravimetric analysis), water resistance (contact angle, swelling), and mechanical properties. Furthermore, from the point of view of the adsorptive capacity of PVA-Ch film against the colorant AO7, both, the percentage removal (Re %) and adsorption capacity (Q) were studied. The adsorption isotherms were analyzed by using different models (Langmuir, Freundlich, Temkin, Redlich-Peterson, or Dubinin-Radushkevich. Pseudo first order, Pseudo second order, Elovich, intraparticle diffusion, as well as the mixed surface reaction and diffusion-controlled kinetic models were tested to evaluate the adsorption kinetics. The effect of different competitive ions was also studied and consecutive adsorption-desorption cycles were carried out to evaluate the regeneration and recycling capacity of the hybrid sorbent.

## 2. Material and methods

### 2.1. Reagents

Chitosan flakes from Sigma Aldrich (St.Louis, MO, USA) with a molecular weight of  $2.83 \times 10^5$  (SD =  $0.56 \times 10^5$ ) g/mol and deacetylation degree of 79.5% (SD = 2.7) were used. Poly(vinyl alcohol) with a degree of hydrolysis of 98% and molecular weight of  $7.8 \times 10^4$  g/mol supplied from Elvanol T-25 was used. Acetic acid, sodium hydroxide, and hydrochloric acid were acquired by Anedra (Buenos Aires, Argentina). Potassium chloride, potassium nitrate, potassium sulfate, and potassium carbonate were supplied by BioPack (Buenos Aires, Argentina). Acid Orange 7 azo dye was provided by Chromeco S.A (Gral. Pacheco, Argentina).

### 2.2. Preparation of hybrid biosorbent films

The biosorbent material formed from hybrid films of the PVA-Ch blend was obtained using a 10% (w/v) solution of PVA and 2% (w/v) Ch. The Ch solution was prepared by dissolving Ch flakes in 1% (v/v) acetic and PVA was solubilized in water at 90°C for 5 h. The filmogenic solution was a blend of PVA-Ch using the proportion 60/40 (w/w) of the polymeric solutions.

The PVA-Ch blend was kept under constant agitation at 300 rev/min using a magnetic hot plate stirrer IKA model RET CV C (IKA Lab, Germany) at 25°C for 8 h. PVA-Ch hybrid films were obtained by the casting technique. For this purpose, the polymeric blend was disposed over rectangular acrylic plates; the amount of polymer solution corresponded to a solids ratio of 16.1 mg/cm<sup>2</sup>. The plates were then dried at 37°C for 24 h using a forced convection oven model DGH-9123A (Shanghai Fengling Lab. Inst. Co., Ltd China) until a constant weight was reached. Before characterization and use, films were conditioned at 20°C and 60% relative humidity (RH).

### 2.3. Thermal curing treatments

Physical stabilization of PVA-Ch hybrid films was carried out by a thermal curing process using a forced convection oven DGH-9123A (Shanghai Fengling Lab. Inst. Co., Ltd China). Two temperatures (120°C and 160°C) and three curing times (1, 3, and 6 h) were tested. After the thermal treatment, the films were stored in airtight containers at 20°C and 65% RH prior to the subsequent tests.

### 2.4. Hybrid biosorbent film characterization

Physical properties of the biosorbent films such as weight loss ( $W_L\%$ ) and swelling degree ( $Sw\%$ ) were determined. A  $2 \times 2$  cm film sample was placed in 50 mL of distilled water and kept under constant agitation in a temperature-controlled orbital shaker MAXQ 400 model SHKA4000-1CE (Barhstead, USA) for 5 h at 25°C. With the obtained results,  $W_L\%$  and  $Sw\%$  were determined according to Equations (1) and (2), respectively.

$$W_L\% = \left( \frac{m_o - m_s}{m_o} \right) \times 100 \quad (1)$$

$$Sw\% = \left( \frac{m_h - m_o}{m_o} \right) \times 100 \quad (2)$$

where,  $m_o$  corresponds to the initial weight of the dry film,  $m_h$  is the weight of the wet film after the test, and  $m_s$  is the weight of the dry film at the final time.

The surface hydrophobicity (contact angle (CA)) of the material at room temperature was determined with a Ramé-Hart Model 550 goniometer (Ramé-Har Instrument Co., United States).

Film color was measured by using a Minolta colorimeter model CR 400 Series (Minolta Chroma Co, Japan). The CIELab scale was used to measure lightness ( $L^*$ ) and the chromatic coordinates/parameters  $a^*$  and  $b^*$ . For each film, before and after the thermal curing process, the browning index (BI) was calculated by Equation (3) [45].

$$BI = \frac{\left[ 100 \left( \frac{a^* + 1.75L}{5.645L + a^* - 3.012b^*} - 0.31 \right) \right]}{0.172} \quad (3)$$

Mechanical properties were established by tensile testing using a TA.X texturometer model T2i (Stable Micro Systems, England), equipped with an A/TG tensile gripping system at a constant rate (0.5 mm/s). The tensile testing allowed obtaining curves of tensile force (MPa) vs deformation (mm). These variables were analyzed using Texture Expert V.1.22 software calculating the tensile stress (E) and elongation % ( $\epsilon_r\%$ ).

The interactions between the functional groups of the films were analyzed through Fourier transforms infrared spectroscopy technique using a Thermo Nicolet FTIR spectrometer Model iS10 (ThermoScientific, USA), coupled to a diamond attenuated total reflection (ATR) accessory (nominal angle of incidence = 42°). ATR-FTIR spectra were obtained in absorbance mode with 4 cm<sup>-1</sup> spectral resolution and 32 scans in the range of 400–4000 cm<sup>-1</sup> and analyzed using Omnic 8 software (ThermoScientific). The surface and cross-sectional morphology of the biosorbent films was observed by scanning electron microscopy (SEM) using an FEI microscope model Quanta 200 (The Netherlands).

Thermal analysis of the material was carried out using thermogravimetric analysis (TGA) and modulated differential scanning calorimetry (MDSC). TGA was conducted in a thermogravimetric analyzer STA Thermo Plus model EVO2 (Rigaku, Japan) at a rate of 10°C/min until 700°C. Dynamic N<sub>2</sub> inert atmosphere and aluminum capsules were used. MDSC was carried out using a controlled DSC model Q100 (TA Instruments, New Castle, Delaware, USA) and the heating rate was 10°C/min until 300°C.

### 2.5. Batch adsorption tests for the removal of the Acid Orange 7 dye

The adsorption experiments were carried out in batch tests evaluating different factors such as the effect of the thermal treatment on the material, the dosage of the adsorbent material, and the pH of the medium. For these cases, the removal percentage

(Re%) and the adsorption capacity (Q) achieved by the hybrid biosorbents were calculated using Eqs. (4) and (5), respectively.

$$Re\% = \frac{C_i - C_t}{C_i} \times 100 \quad (4)$$

$$Q = \frac{(C_i - C_t)}{W} \times V \quad (5)$$

where,  $C_i$  is the initial concentration of the dye in the solution (mg/L),  $C_t$  is the concentration at a given time after starting the process;  $V$  is the volume of the solution (L) and  $W$  is the film weight (g). When the adsorption equilibrium was reached,  $C_t$  was replaced by  $C_e$  (dye concentration at equilibrium (mg/L)), in Eqs. (4) and (5).

Acid Orange 7 (AO) azo dye was selected (CAS Number 633-96-5; MW = 350.32 g/mol) for the experimental assay. The experimental conditions to evaluate the effect of thermal curing in the adsorption process were:  $V = 10$  mL,  $C_i = 45$  mg/L, agitation speed: 150 rev/min,  $T = 25^\circ\text{C}$  and adsorbent dose =  $0.8\text{ g film/L}_{\text{dye solution}}$ ; for these tests, the pH of the medium was adjusted to 4.0 since in previous studies it was reported that Ch-based materials present the maximum Re% at this pH [46,47].

After selecting the most appropriate thermal curing procedures, the effects of different experimental sorption conditions, such as adsorbent dose, pH values, and temperature variation, were evaluated. Adsorbent doses ranged from 0.6 to 18.2  $\text{g film/L}_{\text{dye solution}}$ ; in all experiments, pH was adjusted with hydrochloric acid and 0.1 N sodium hydroxide ranging from 2.5 to 11. The experimental conditions were:  $V = 10$  mL,  $C_i = 25$  mg/L, agitation speed: 150 rev/min, and  $T = 25^\circ\text{C}$ . In addition, the temperature ranged from 25 to  $45^\circ\text{C}$  for the following experimental conditions:  $V = 10$  mL,  $C_i = 400$  mg/L, agitation speed 150 rev/min.

For the adsorption tests, the ionic strength was controlled using a potassium chloride solution (1 mM), and the electrical conductivity was determined with a Seven conductivity meter model Multi S47 (Mettler Toledo, Switzerland) equipped with a cond probe InLab model 738 ISM (InLab, USA). The final dye concentration was recorded by using a UV-visible Spectrophotometer Hach model DR 2800 (Hach, USA) at a wavelength of 484 nm.

## 2.6. Study of equilibrium isotherm and adsorption kinetics

To analyze the equilibrium isotherm and adsorption kinetics, the adsorption capacity (Q) of the PVA-Ch hybrid biosorbent was determined by Eq. (5). When the test times were long and equilibrium was reached Q was denoted as  $Q_e$ .

The equilibrium adsorption isotherms of AO7 onto PVA-Ch films were determined using different initial concentrations of AO7 ( $C_i = 45$ –1100 mg/L). The results were analyzed using Langmuir, Freundlich, Redlich-Peterson (RP), and Dubinin-Radushkevich (DR) models.

To analyze the results of the adsorption kinetics at 298 K, pseudo-first-order (Ps1), pseudo-second-order (Ps2), Elovich, and mixed diffusion-adsorption (MSR-DK) models were used. The experimental conditions to determine the isotherm and kinetics were: an initial concentration of AO7 of 45 mg/L, 150 rev/min, and a volume of 10 mL.

## 2.7. Effect of competitive ions

The effect of different competitive ions and changes of ionic strength on the adsorption process were evaluated. The tested ions were  $\text{Cl}^-$ ,  $\text{NO}_3^-$ ,  $\text{SO}_4^{2-}$ , and  $\text{HCO}_3^-$  at a concentration of 25 mmol/L. In all cases, the solutions were prepared with Milli-Q water. The  $C_i$  of the dye was 170 mg/L and the salts used were potassium chloride

(KCl), potassium nitrate ( $\text{KNO}_3$ ), potassium sulfate ( $\text{K}_2\text{SO}_4$ ), and potassium carbonate ( $\text{KCO}_3$ ).

## 2.8. Regeneration and reuse of biosorbent hybrid material

Five consecutive desorption/adsorption cycles were performed. During the desorption (regeneration) step, PVA-Ch film saturated with the dye was placed in contact with Milli-Q water (10 mL) under alkaline conditions ( $\text{pH} = 12$ ). The regenerated PVA-Ch film was dried in a forced convection oven at  $37^\circ\text{C}$  until reaching a constant weight. In the adsorption stage, the regenerated PVA-Ch film was kept in contact with the AO7 solution ( $C_i = 300$  mg/L;  $V = 10$  mL;  $T = 25^\circ\text{C}$ ). Five adsorption/desorption cycles were completed. At the end of each stage, the adsorbent film was characterized by mechanical properties ( $E$ ,  $\epsilon_r\%$ ), contact angle (CA), and browning index (BI).

## 2.9. Statistical analysis

Analysis of variance (ANOVA) was performed using InfoStat software (National University of Cordoba, Argentina); means were compared using Fisher's LSD test (95% confidence level ( $p < 0.05$ )). Origin-Pro 8 software (Origin Lab Corporation, Northampton, MA, U.S.A.) was used to evaluate the different mathematical models describing adsorption kinetics, thermodynamics, and equilibrium isotherms. The goodness of fit of the nonlinear models was performed by analyzing the mean percentage error (MAPE), the coefficient of determination ( $R^2$ ), and the chi-square error distribution parameter ( $\chi^2$ ).  $\chi^2$  and MAPE were determined using Eqs. (6) and (7), respectively, where  $y_e$  is the experimental value and  $y_p$  is the predicted value.

$$MAPE = \frac{\sum |(y_e - y_p) / y_e|}{n} \times 100 \quad (6)$$

$$\chi^2 = \sum \frac{(y_e - y_p)^2}{y_p} \quad (7)$$

# 3. Results and discussion

## 3.1. Effect of thermal curing on physical properties of hybrid films
















PVA-Ch films with a thickness of 137.7  $\mu\text{m}$  ( $\text{SD} = 24.1$ ) were obtained. These films were exposed to thermal curing treatments at different temperatures ( $120^\circ\text{C}$  and  $160^\circ\text{C}$ ) and times (1, 3, and 6 h). Table 1 shows the results of the different parameters obtained from the characterization of the properties and the photographs of the samples.

Aycan et al. [48] reported that 60/40 (PVA-Ch) ratios are the most appropriate to obtain materials to retain film structure in solution and film flexibility.  $S_w\%$  and  $W_L\%$  obtained for PVA-Ch control film (without heat treatment) showed complete dissolution of the material after 5 h of testing which makes it undesirable for its use as biosorbent. In contrast, when the films were submitted to a thermal treatment,  $W_L\%$  decreased showing the lowest values for a curing temperature of  $160^\circ\text{C}$  irrespective of the treatment time (Table 1). Meanwhile,  $S_w\%$  exhibited the lowest values for a temperature-time combination of  $160^\circ\text{C}$ -6h (Table 1). These results suggested that the polymeric structure of the hybrid matrix was drastically modified by the thermal curing process.

The physical stability (insolubilization) of the hybrid material and the swelling decrease after thermal treatments could be explained due to hydrogen bond-type interactions between PVA

**Table 1**

Characterization of hybrid films without heat treatment (PVA-Ch) and after the curing at 120°C and 160°C, showing contact angle (CA), swelling (Sw%), weight loss (W<sub>L</sub>%), tensile strength (E), elongation (ε<sub>r</sub>%), browning index (BI), removal percentage (Re%), and adsorption capacity (Q).

	CA (°)		Sw%	W <sub>L</sub> %	E (MPa)	ε <sub>r</sub> %	BI	Film photography	Adsorption properties		
									Re%	Q (mg/g)	
PVA/Ch	78.1 (0.4) <sup>g</sup>		—	—	41.9 (3.9) <sup>a</sup>	114.0 (6.2) <sup>e</sup>	8.05 (1.43) <sup>a</sup>		—	—	
120°C	1 h	77.9 (3.9) <sup>e</sup>		621 (65) <sup>e</sup>	12.1 (3.9) <sup>c</sup>	57.3 (9.8) <sup>b</sup>	98.0 (9.6) <sup>d</sup>	20.50 (0.63) <sup>b</sup>		80.4 (1.8) <sup>c</sup>	116.7 (4.9) <sup>c</sup>
	3 h	73.3 (4.4) <sup>e</sup>		442 (11) <sup>d</sup>	6.7 (0.8) <sup>b</sup>	57.6 (4.5) <sup>b</sup>	91.5 (9.7) <sup>c</sup>	35.63 (2.14) <sup>c</sup>		82.3 (0.8) <sup>c</sup>	119.4 (5.8) <sup>c</sup>
	6 h	68.3 (5.8) <sup>d</sup>		347 (14) <sup>d</sup>	8.7 (0.3) <sup>b</sup>	58.9 (9.6) <sup>b</sup>	89.5 (9.9) <sup>c</sup>	88.34 (4.37) <sup>d</sup>		90.2 (1.2) <sup>d</sup>	130.9 (6.9) <sup>d</sup>
160°C	1 h	59.8 (6.6) <sup>c</sup>		75.4 (2.1) <sup>b</sup>	0.017 (0.008) <sup>a</sup>	53.1 (9.6) <sup>b</sup>	80.6 (8.2) <sup>b</sup>	107.62 (5.10) <sup>e</sup>		91.1 (1.4) <sup>d</sup>	132.3 (9.2) <sup>d</sup>
	3 h	49.8 (1.3) <sup>b</sup>		79.4 (9) <sup>c</sup>	0.018 (0.003) <sup>a</sup>	58.3 (6.0) <sup>b</sup>	78.2 (4.9) <sup>b</sup>	195.59 (7.33) <sup>f</sup>		60.3 (0.2) <sup>b</sup>	87.6 (1.6) <sup>b</sup>
	6 h	37.1 (3.2) <sup>a</sup>		47 (7) <sup>a</sup>	0.015 (0.001) <sup>a</sup>	46.0 (5.0) <sup>a</sup>	16.7 (6.2) <sup>a</sup>	273.39 (43.58) <sup>g</sup>		44.9 (0.4) <sup>a</sup>	65.2 (1.3) <sup>a</sup>

Reported values correspond to the mean, in parentheses standard deviation.

<sup>a,g</sup>Different lower case letters indicate significant differences between column values (Fisher LSD comparison test,  $p < 0.05$ ).

and Ch. Thermal treatment is efficient in comparison to other types of chemical crosslinkers. Çay et al. [49] informed that for PVA-Ch nanofibers treated for 3 h at 180°C, the Sw% was 310 %. This value is lower than those obtained with other crosslinkers such as methanol (Sw% = 700) and glutaraldehyde (Sw% = 800), and there was no significant weight loss of the material. Xianda and Anlai [50] informed that for PVA films, the thermal treatment generated a decrease in the hygroscopicity of the material due to a decrease in the permeability of water vapor. Aycan et al. [48] found that the physical treatment generated a greater decrease in Sw% for a curing temperature of 160°C compared to the chemical crosslinking with genipin.

The hybrid blend is composed of two polymers, Ch which is insoluble in water at neutral pH, and highly hydrophilic PVA, therefore the surface hygroscopicity of the material would be largely provided by PVA [51]. In the case of the control film (PVA-Ch without thermal treatment), a higher contact angle (CA) was obtained compared to the films submitted to thermal curing treatments ( $p < 0.05$ ). Given that CA is a surface property, the nature of the interaction between the film and the water droplet was involved. The thermal treatment may contribute to the reorientation of the polar functional groups onto the surface due to the polymeric rearrangement reactions. The decrease of CA in PVA-Ch films was due to the existence of polar groups on the surface of the materials. According to Chen et al. [52], the PVA-Ch films with a higher PVA content showed a lower CA.

Table 2 shows photographs taken at different times of the CA evolution. In the case of films without thermal treatment, a decrease in the CA was obtained after 30 min of testing, because this material increased its humectability. Moreover, it was found that between 60 and 90 min, the drop of water generated the collapse of the material surface due to a solubilization process. On the contrary, the CA of the sample previously exposed to 160°C-1h did not change in the first 30 min ( $p < 0.05$ ) but after 60 min swelling of the film was observed, indicating that the curing treatment helped to prevent the structural collapse of the hybrid film.









Tensile tests were performed on PVA-Ch control and PVA-Ch films submitted to the curing process. From the mechanical profiles, the tensile stress (E) and percent elongation (ε<sub>r</sub>%) of the samples were calculated. The results are presented in Table 1. Some authors have mentioned that the PVA-Ch blend generated films with higher tensile strength compared to control PVA-Ch films [53,54]. This phenomenon was due to the intermolecular interactions between the polymeric chains of the free hydroxyl groups (-OH) of PVA, where hydrogen is an electron acceptor, and the amino protonated (-NH<sub>3</sub><sup>+</sup>) (as electron donors) and hydroxyl groups from Ch [55].

On the other hand, the addition of PVA provided elastic properties to the rigid Ch film. In the case of control PVA-Ch, the highest value of ε<sub>r</sub>% was obtained, which decreased as the intensity of the thermal treatment increased. In this way, in films submitted to the treatment of 160°C-6 h, ε<sub>r</sub>% presented the lowest value ( $p < 0.05$ ) since the thermal over-treatment established polymeric interactions between the constituents resulting in a rigid material. The intensity of the thermal curing led to an increase in E. When crosslinking occurs, the reduction of the chain mobility forms a three-dimensional network with greater polymeric interactions [48] and the intermolecular forces became dominant. In the case of the highest curing intensity (160°C-6 h), both E and ε<sub>r</sub>% significantly diminished as a consequence of possible degradation of the matrix.

Using the chromatic parameters, the BI values calculated for the samples are presented in Table 1. As the intensity of the treatment increased, the BI increased, indicating that the physical appearance of the film changed becoming browner compared to the PVA-Ch control film. This change occurred because of the browning reactions and can be attributed to the compounds present in the biopolymer matrices and the high temperatures applied. The photographs (Table 1) show the physical appearance of the hybrid films after the thermal curing process. Çay et al. [49] reported that the alteration of the ordering of the polymeric chains increased with the treatment time leading to the breaking of the polymeric chains when

**Table 2**

Photographs obtained of the surface interaction between the water droplet and the hybrid film without heat treatment (PVA-Ch) and exposed to thermal curing at 160°C and 1 h. Reported values correspond to the mean, in parentheses standard deviation. Different lower case letters indicate significant differences between row values (Fisher comparison test LSD,  $p < 0.05$ ). ND= No detected.

	t = 0	t = 30 min	t = 60 min	t = 90 min
PVA-Ch				
	78.1° (0.4) <sup>a</sup>	48.2° (0.1) <sup>b</sup>	ND	ND
160°C-1h				
	45.1° (0.05) <sup>a</sup>	44.8° (0.05) <sup>a</sup>	ND	ND

the degradation of the network was reached. This finding supported the obtained results of the mechanical properties.

### 3.2. Microstructural and morphology characterization of the hybrid film

#### 3.2.1. ATR-FTIR analysis

ATR-FTIR spectra (Fig. 1-a) of the hybrid films were obtained, before and after the thermal curing process. In all spectra, the characteristic peak of hydrogen bridges established among the hydroxyl groups of the C2 and C3 of chitosan and the hydroxyl groups of PVA was observed at 3252  $\text{cm}^{-1}$  [56,57].

The PVA-Ch control film showed bands at 1646  $\text{cm}^{-1}$  attributed to the stretching of the C=O carbonyl group of amide-I and the vibrations of amide-I, 1562  $\text{cm}^{-1}$  assigned to the bending vibration of the amide-II group, which overlaps with the bending of the amino group at 1549  $\text{cm}^{-1}$ . At 1414  $\text{cm}^{-1}$  the signal characteristic of the interactions between the PVA and Ch affecting the C–H vibrational motion of the PVA [58] band at 1142  $\text{cm}^{-1}$  associated with the crystalline structure of PVA were also observed [49].

The ATR-FTIR spectra of the PVA-Ch films, after the thermal curing process (Fig. 1-a), showed significant changes regarding the control film. The characteristic peaks at 2949  $\text{cm}^{-1}$  and 2854  $\text{cm}^{-1}$  were due to the asymmetric and symmetric stretching vibration of the  $-\text{CH}_2$  group of the PVA-Ch blend. As the curing time and temperature increased, the signal at 2949  $\text{cm}^{-1}$  became more pronounced and shifted to 2913  $\text{cm}^{-1}$ .

The peak at 1745  $\text{cm}^{-1}$  was assigned to the physical cross-linking of PVA [59]. This signal characteristic of the non-

hydrolyzed ester bonds of the polyvinyl acetate chain (C=O) experienced a break during the curing process, decreasing for the 160°C-6h treatment (Fig. 1-a).

The band at 1562  $\text{cm}^{-1}$ , attributed to the bending vibration of the amide-II group of Ch, decreased during the curing treatment indicating that the amino groups of the chitosan were not present. Similar results have been reported by Rivero et al. [60].

The bands located at 1424  $\text{cm}^{-1}$  and 1336  $\text{cm}^{-1}$  corresponding to the C–H vibrational motion [56] and the  $-\text{CH}_2$  linking  $-\text{OH}$  group [61], shifted toward lower wavelengths due to hydrogen bonding between the Ch and the PVA [56].

The signal at 1147  $\text{cm}^{-1}$  attributed to the stretching of groups that make up the crystalline structure of PVA [62] became more evident at higher temperatures. Meanwhile, the reduction of the signal intensity and broadening of the peak at 1088  $\text{cm}^{-1}$  was due to the crosslinking of the PVA polymeric network [55].

#### 3.2.2. SEM observation

SEM cross-section micrographs of the films exposed to thermal curing as well as the control film are shown in Fig. 1b–e. Fig. 1–e exhibits the film exposed to the most extreme treatment (160°C for 6 h) showing the complete loss of the porous structure that interconnects the inner part of the material. For this curing condition, the lowest degree of Sw% was obtained (Table 1). Consequently, the prolonged exposure of the material to the curing treatment generated a structural morphology with low interconnectivity without the presence of pores. This fact would explain that both the degree of swelling and water retention were minimal. Characteristics such as no interconnectivity and low degree of swelling are

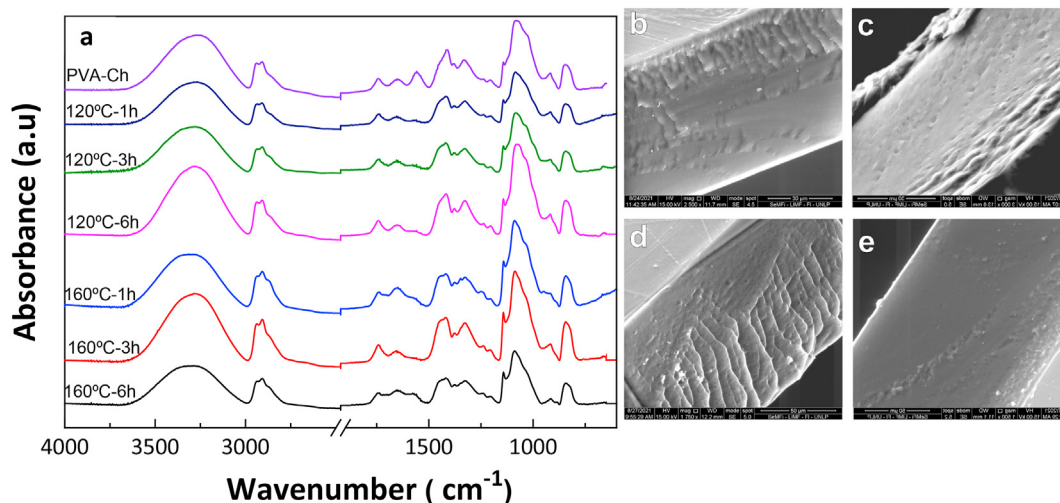


**Fig. 1.** Microstructural and morphology characterization of the hybrid adsorbent film **a.** ATR-FTIR spectra of PVA-Ch films before and after the thermal curing. SEM micrographs obtained from cross-sections of the films: **b.** PVA-Ch control; after thermal curing treatments: **c.** 120°C – 1 h, **d.** 160°C-1h, **e.** 160°C-6h.

not suitable for the generation of polymer-based biosorbents since these materials must have features like a hydrogel in aqueous media to retain the pollutant in the bulk of the material [63].

### 3.3. Effect of thermal curing on the removal process of synthetic dye

The removal of AO7 from PVA-Ch films was evaluated after the physical crosslinking process achieved by the curing treatment. In the case of the control PVA-Ch film, adsorption tests were not carried out because the material without physical crosslinking was completely dissolved. Table 1 shows the adsorption properties (Re% and Q) for the films after being subjected to the curing process, in which it can be observed that the thermal treatment affected the dye removal. Under extreme temperature and time conditions (160 °C and 3–6 h) a lower Re% value was attained compared to the other conditions. In the case of the treatment at 160 °C-1h, the best adsorption performance was comparable to that of 120 °C-6h. It is noteworthy that under these last curing conditions, the material presented a W<sub>l</sub>% higher than 8% (Table 1), indicating that this treatment was not sufficient to give physical stability to the film.

The 160 °C-1h treatment yielded the best adsorption results for AO7 (Re% = 91.1 and Q = 132.3 mg/g). This was the best condition used to generate a physical crosslinking process, because not only this time-temperature combination did not compromise the removal properties but also the adsorbent material showed a controlled swelling. Thus, the diffusion and/or adsorption processes of the dye molecules took place without dissolution in the aqueous medium.

Furthermore, concerning the adsorption results, the morphology observed by SEM (Fig. 1-d) for the 160 °C-1h treatment showed that the material conserved the porous structure, essential in the adsorption processes. This porous morphology was lost in the case of 160 °C-6h (Fig. 1-e), and the material obtained after this treatment presented a poor removal of AO7 of 44.9%.

The decrease of Re% for the film treated at 160 °C-6h indicated that the polymeric network lost the ability to interact with the dye molecules, probably due to the excessive cross-linking of the polymeric networks that did not allow the input of the adsorbate into the film. This characteristic was accompanied by the low Sw% obtained for this film (Sw% = 47%, Table 1). According to Crini et al. [14], in highly cross-linked materials, functional properties such as adsorption capacity decreased.

#### 3.3.1. Thermal analysis of the films

The results obtained by thermogravimetric analysis (TGA) and the first derivative (DTG) (Fig. 2a and b) showed three thermal stages. During the first stage (20°-180 °C), the films submitted to the curing process showed a higher dehydration temperature, compared to the control film (PVA-Ch). The latter experienced a higher weight loss (17.4%) compared to treated samples (8.1% for 160 °C-1h) because the substitution of hydrogen bonds by interactions between intra-polymeric –OH radicals [49] reduced the water content.

The second thermal stage (180°-480 °C) corresponded to the degradation of the polymeric material and the generation of the corresponding decomposition residues [64] such as compounds with aldehyde and alkene functional groups, which would eventually lead to the formation of a vinyl ester and polyene residues by structural rearrangement [52,65]. The third stage was associated with the total degradation of the polymers and the residual compounds generated in the second stage, finally forming carbon and hydrogen. The maximum weight losses were 97.1 and 96.5% for the control and treated samples, respectively (Fig. 2-a).

Peaks of DTG curves indicate the temperatures of the maximum slope of the three stages as shown in Fig. 2-b and Table 3. In the

second and third stages, the peaks had higher intensity, which according to Rana et al. [66] was a signal of higher thermal stability of the matrix. In this stage, the DTG curves showed a maximum decomposition peak at 513 °C for PVA and samples subjected to 160 °C-1 h.

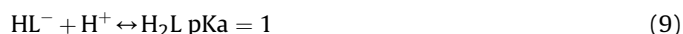
The modulated differential scanning calorimetry (MDSC) allowed visualizing the glass transition temperature (T<sub>g</sub>) of the material from the reversible heat flow curves (Fig. 2-c). The T<sub>g</sub>, after the curing treatment, underwent a shift to a higher temperature (p < 0.05) probably due to the crosslinking process supporting the results obtained by ATR-FTIR and TGA.

### 3.4. Study of the adsorption of the dye AO7: effect of adsorbent dose, pH, and temperature

According to the results of structural characterization, physical stability in an aqueous medium, and adsorption performance, the film treated at 160 °C for 1 h was selected for further analysis. Fig. 3 shows the effects of the adsorbent dose, pH value of the medium, and temperature containing the colorant (V = 10 mL, C<sub>i</sub> = 25 mg/L) on the adsorption capacity (Q) and the removal percentage (Re%) in a batch test. The dose selected for the adsorption experiments was 0.8g film/L<sub>dyesolution</sub> because, at this conditions, the highest removal of the AO7dye (Fig. 3-a) was reached (Re% = 95.1% (SD = 0.4)) in comparison to 0.6 g/L (Re% = 85.1% (SD = 1.8)).

Fig. 3-b shows that pH is a critical parameter in the removal process and affects the adsorption capacity of the material, hence as pH decreased the dye removal increased. At pH 2.5, the capacity of the material increased significantly compared to the other pH values (p < 0.05). At this condition, the film did not experience weight losses (W<sub>l</sub>% = 0.007 at pH = 2.5) indicating the cross-linking of the polymeric network and the stabilization of the material under acidic conditions. In this medium, it would expect the dissolution of the material due to the pK<sub>a</sub> of chitosan (pK<sub>a</sub> = 6.3–6.5) [24]. Furthermore, at acidic pH, chitosan has highly protonated amino groups (NH<sub>3</sub><sup>+</sup>), which generates the appropriate conditions for the interaction with the anionic groups of the dye (sulfonate and hydroxyl groups).

The pK<sub>a</sub>s of the dye AO7 are 10.6 and 1 [67], indicating that in an aqueous solution, it can exist in three species: i) at pH lower than 1 the molecule is doubly protonated (H<sub>2</sub>L), ii) in pH range between 1 and 10.6 the molecule is mono protonated (HL<sup>-</sup>), and iii) at pH higher than 10.6 the molecule is not protonated (L<sup>2-</sup>). The equilibrium speciation of AO7 is given by:



At pH = 2.5, when the maximum adsorption occurred (Fig. 3-b), the predominance of H<sub>2</sub>L and HL<sup>-</sup> species may occur. Thus, the electrostatic attraction between the dye molecules and the functional groups involved in the removal of the sorbent material increased [67]. The decrease in the removal percentage at alkaline pH values was due to the coexistence of two facts, the amine groups of chitosan are deprotonated (NH<sub>2</sub>). This phenomenon can be explained by the competition between the negative charges provided by dye molecules and hydroxyl groups for the positive sites of the sorbent material under alkaline conditions.

The photographs in Fig. 3-c show the physically crosslinked hybrid film before and after the AO7 adsorption assay at pH = 2.5, acquiring the color of the dye in the solution. In addition, after the adsorption assay, the material exhibited physical integrity, retained its structure, and did not show weight loss.

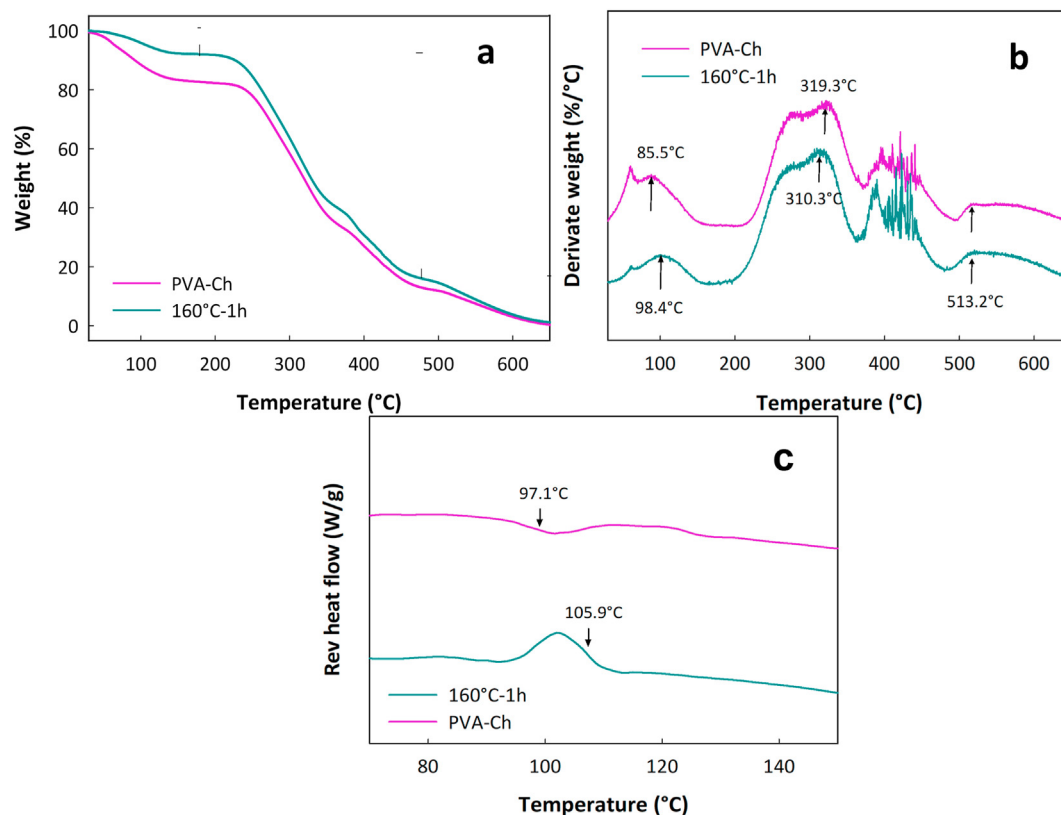


**Fig. 2.** Thermal behavior of the hybrid film without treatment (PVA-Ch) and after the treatment at 160°C-1h. The results correspond to: **a.** thermogravimetric analysis (TGA), **b.** first derivative (DTG) of the TGA results, **c.** reversible heat flow in MDSC.

**Table 3**

Weight losses obtained from TGA and maximum temperatures from DTG of hybrid films corresponding to the different stages of the degradation process.

	I stage (20–180°C)		II stage (180–480°C)		III stage (480–620°C)		Residual weight (%)
	T <sub>max</sub> (°C)	Weight loss (%)	T <sub>max</sub> (°C)	Weight loss (%)	T <sub>max</sub> (°C)	Weight loss (%)	
PVA-Ch	88.5 <sup>a</sup>	17.4 <sup>c</sup>	310.3 <sup>a</sup>	71.0 <sup>a</sup>	513.2 <sup>a</sup>	8.7 <sup>b</sup>	2.9 <sup>a</sup>
160°C-1h	102.4 <sup>b</sup>	8.1 <sup>b</sup>	319.3 <sup>b</sup>	76.4 <sup>b</sup>	513.2 <sup>a</sup>	12.0 <sup>c</sup>	3.5 <sup>a</sup>
160°C-1h + AO7	107.5 <sup>c</sup>	7.0 <sup>a</sup>	345.2 <sup>c</sup>	77.1 <sup>b</sup>	–	4.0 <sup>a</sup>	11.9 <sup>b</sup>

<sup>a,b</sup> Different lower case letters indicate significant differences between column values (Fisher LSD comparison test, p < 0.05).

Previous studies have demonstrated that crosslinking processes of chitosan generate stable hydrogels in an acid medium improving the adsorption properties of the material. Chitosan hydrogels, ionically crosslinked by oxalic acid at pH 2.5, achieved the highest Q and Re% for the adsorption of the azo-dye Reactive Red 195 [68]. Physical crosslinking (thermal curing) has not been reported so far to generate a polymeric stabilization of matrices composed of Ch and PVA, making it possible to obtain materials with better adsorbent properties and physical stability at acidic pH. Similar results were informed for AO7 removal by polypyrrole/nanosilica composite [69], kenyan tea pulps in the granular form [70], aluminum oxide nanoparticles [71], and sugarcane bagasse modified with cetylpyridinium bromide [67].

Fig. 3-d shows the results of the adsorption temperature at the pH of maximum adsorption (pH = 2.5, Fig. 3-b). The adsorption process was less efficient with increasing temperature due to the decrease in Q and Re%. Akazdam et al. [72] obtained similar results for the adsorption of AO7 onto Amberlite FPA-98 resin. In the case of chitosan adsorbent films, Dotto et al. [73] reported the same tendency for the adsorption of the dye Acid Red 18.

### 3.5. Adsorption kinetics

Different pH values (2.5 and 4.0) were studied to know the effect on the adsorption kinetics. The experimental results were analyzed mathematically using pseudo-first-order (Ps1 Order), pseudo-second-order (Ps2 Order), Elovich, intraparticle diffusion, and mixed diffusion and adsorption (MSR-DCK) models applying non-linear regressions. The equations of each model are shown in Table 4.

Fig. 4-a shows the results of the adsorption kinetics, in which it can be observed that at pH = 2.5, the adsorption capacity at equilibrium, Q<sub>e</sub> increased by 73.3% compared to the process at pH = 4.0; the corresponding values being 348.3 mg/g and 93.7 mg/g, respectively. These results showed that the developed material presented physical and chemical stability in a highly acid medium without weight loss. The pH did not affect the time to reach the saturation and equilibrium conditions which were reached after contact time.

Taking into account the models applied, the best fitting of the experimental data was obtained by using the Ps.1 order model. Table 4 shows the parameters of each evaluated model. According



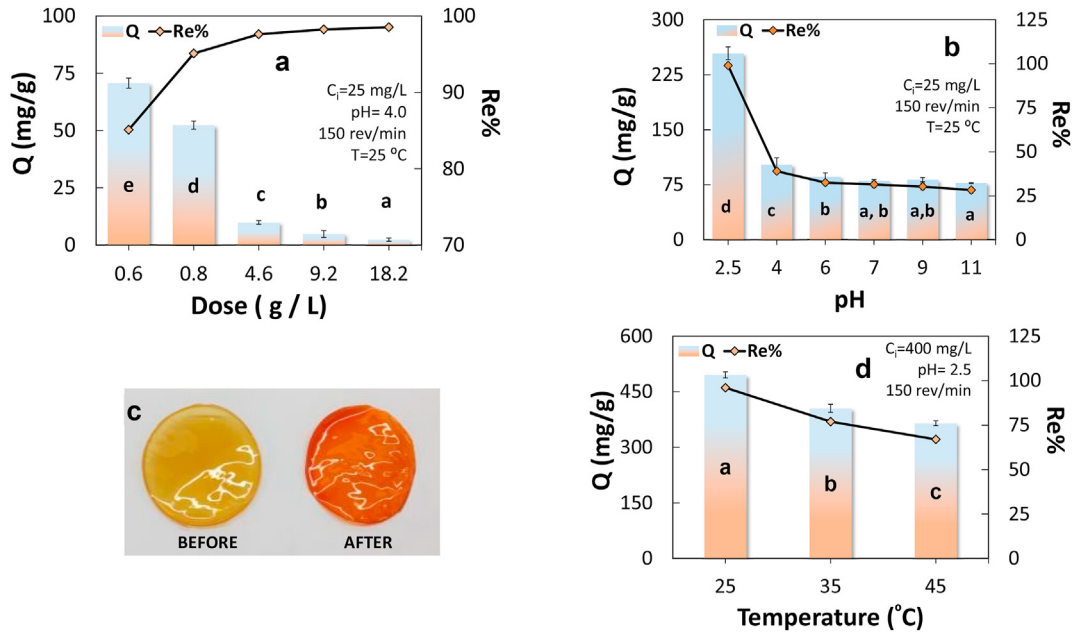


**Fig. 3.** Adsorption removal of AO7 dye in batch test. Effect of: **a.** adsorbent dose, **b.** pH on adsorption capacity (Q) and removal percentage (Re%), **c.** photographs before and after the adsorption process of the crosslinked hybrid films. **d.** Effect of temperature variation on Q and Re%. Different letters in the Q bars indicate significant differences among the samples (Fisher LSD comparison test,  $p < 0.05$ ).

**Table 4**

Equations and parameters of the Acid Orange 7 adsorption kinetic models using PVA-Ch films crosslinked by thermal process. Conditions: C<sub>i</sub> = 300 mg/L; T = 25 °C; 150 rev/min.

MODEL		pH condition		
		pH = 2.5	pH = 4.0	
Ps. 1 order $Q_t = Q_e(1 - \exp^{-k_1 t})$ (10)	<b>Q<sub>e</sub></b>	348.3	89.0	
	<b>k<sub>1</sub></b>	0.54	0.33	
	$\chi^2$	34	23	
	<b>R<sup>2</sup></b>	0.99	0.98	
	<b>MAPE</b>	0.07	2.94	
	<b>Q<sub>e</sub></b>	380.5	102.1	
Ps. 2 order $Q_t = \frac{k_2 Q_e^2 t}{1 + k_2 Q_e t}$ (11)	<b>k<sub>2</sub></b>	0.0018	0.0037	
	$\chi^2$	341	20	
	<b>R<sup>2</sup></b>	0.97	0.98	
	<b>MAPE</b>	2.58	6.01	
	<b>β<sub>E</sub></b>	0.015	0.044	
	<b>α<sub>E</sub> × 10<sup>5</sup></b>	60.7	60.8	
Elovich $Q_t = \frac{1}{\beta_E} \ln(1 + \alpha_E \beta_E t)$ (12)	$\chi^2$	43	42	
	<b>R<sup>2</sup></b>	0.95	0.90	
	<b>MAPE</b>	58.3	8.30	
	Intraparticle diffusion $Q_t = k_i t^{0.5} + c$ (13)	<b>k<sub>i</sub></b>	51.9	17.1
		<b>C<sub>1</sub></b>	123.6	14.3
		$\chi^2$	2974	126
<b>R<sup>2</sup></b>		0.72	0.87	
<b>MAPE</b>		8.54	12.19	
<b>k × 10<sup>-2</sup></b>		1.06	0.0964	
MSR-DCK $Q_t = Q_e \frac{\exp(a \cdot t + b \cdot t^{0.5}) - 1}{(w_{eq} \cdot \exp(a \cdot t + b \cdot t^{0.5}) - 1)}$ (14)	<b>τ</b>	0.05	0.006	
	$\chi^2$	156	28	
	<b>R<sup>2</sup></b>	0.98	0.97	
	<b>MAPE</b>	21.2	5.13	

Units of the parameters used in the kinetic models.

**t:** Time [min] **Q<sub>e</sub>:** Adsorption capacity at equilibrium [mg/g] **k<sub>1</sub>:** Constants of the first order adsorption [1/min].

**k<sub>2</sub>:** Constants of the second order adsorption [g/mg · min].

**α<sub>E</sub>:** Initial adsorption rate [mg/g · min] **β<sub>E</sub>:** Related to the surface coverage and activation energy [mg/g].

**k<sub>i</sub>:** Intraparticle diffusion [mg/(g · min<sup>0.5</sup>)] **c:** Velocity model coefficient transport [mg/g].

**k:** Constants of the MSR-DCK model [L/mg · min] **τ:** Time of the process MSR-DCK model [min].

**a:** MSR-DCK model coefficients [mg/L] **b:** MSR-DCK model coefficients [1/min]

**w<sub>eq</sub>:** Relative equilibrium uptake.

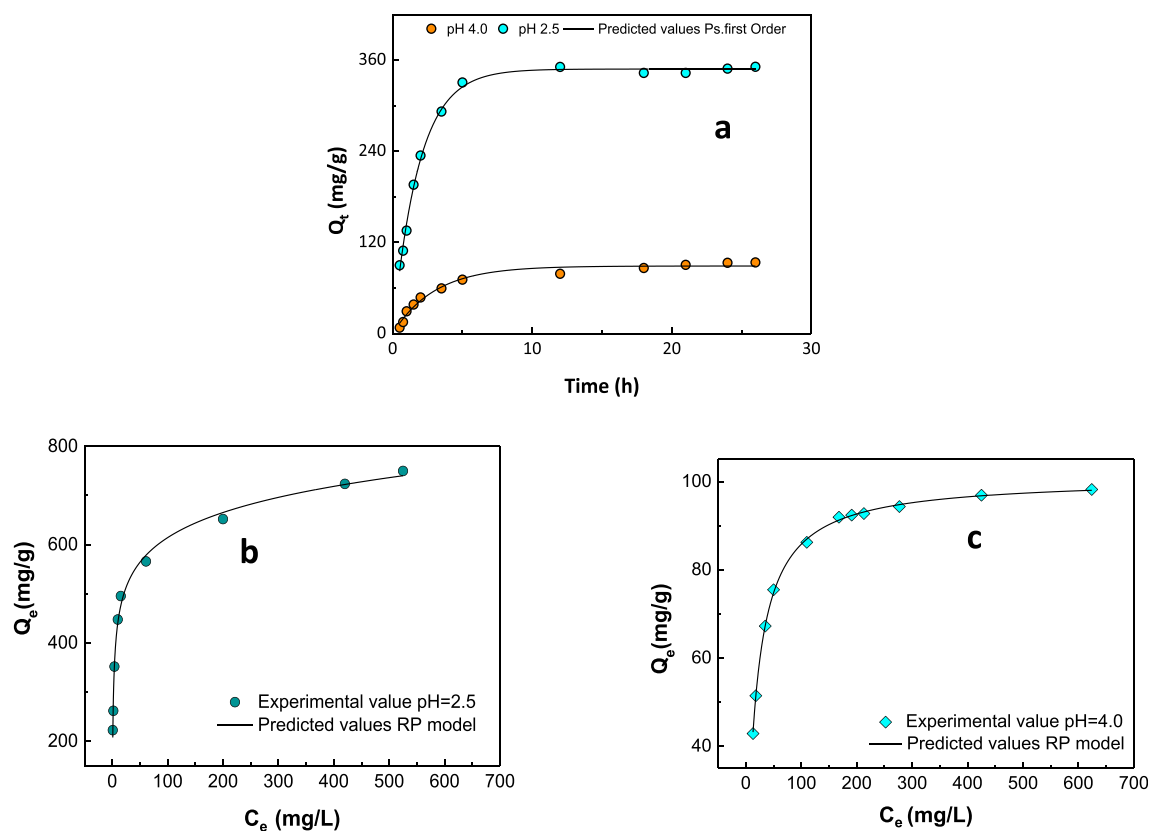


**Fig. 4.** Experimental (dots) and predicted (lines) results for the adsorption of Acid Orange 7 dye at different pH using PVA-Ch sorbent films crosslinked at 160°C-1h: **a.** adsorption kinetics and isotherms at **b.** pH = 2.5 and **c.** pH = 4.0.

to Gupta et al. [10], the Ps.1 order model was successfully used to fit the experimental results of AO7 adsorption of bottom ash and deoiled soya. Wu et al. [74] reported that this model fits the adsorption of methylene blue using chitosan/cellulose nanofibers adsorbent films.

### 3.6. Adsorption isotherms

Non-linear regressions of different adsorption isotherm models (Langmuir, Freundlich, Redlich-Peterson (RP), and Dubinin-Radushkevich (DR) were tested (Table 5). The adsorption isotherms were analyzed for pH values of 2.5 and 4.0.

By applying the Langmuir model (Eq. 15, Table 5), the maximum adsorption capacity ( $Q_m$ ) of the hybrid film (present work) was 678 mg/g at pH 2.5 and 273 K. Several authors have reported  $Q_m$  for AO7 dye removal. According to the reported results,  $Q_m$  of different adsorbents materials in decreasing order were: 666 mg/g (303 K, pH = 3.0) for granular activated carbon from spent coffee/calcium-alginate beads [13], 486 mg/g (298K, pH = NR) for Mg–Al layered double hydroxide composite [12], 356 mg/g (298K, pH = 2.0) onto graphene-cetyl trimethyl ammonium bromide [8], 32.1 mg/g (298 K, pH = 3.0) by using ZnO nanoparticles [75], and 12.5 mg/g (303 K, pH = 2.0) for bottom ash [10]. Thus adsorption results for the developed PVA-Ch films crosslinked by thermal treatment showed the highest value of  $Q_m$  (0.678 mg/g).

The heterogeneity factor ( $n$ ) determined using the Freundlich model (Eq. 16, Table 5) indicated the favorability of the adsorption process. If  $n < 1$ , the adsorption process is poor and unfavorable, while  $n > 1$  indicates favorable adsorption conditions [76]. As can be seen in Table 5, the parameter  $n$  calculated for all the cases indicated that the process was favorable.

The DR model assumes two possible mechanisms (physical or chemical) to explain the adsorption process; Eq. 17 in Table 4 represents this model, where  $e$  (kJ/mol) is Polanyi's potential,  $Q_{DR}$  is the adsorption capacity from the DR model, and  $B_{DR}$  is the constant related to the adsorption energy.  $e$  is calculated using Eq. 17-1 where  $R$  represents the gas constant ( $8.314 \times 10^{-3}$  kJ/K.mol) and  $T$  is the absolute temperature (K). From the value of  $B_{DR}$  (determined by regression Eq. 17) it was possible to calculate the average free adsorption energy ( $E$ , kJ/mol) using Eq. 17-2, where  $E$  defines the mechanism of adsorption: chemisorption ( $E > 8$  kJ/mol) or physisorption ( $E < 8$  kJ/mol) [77].

The RP model is described in Eq. 18 (Table 5), where  $K_{RP}$  (L/g) and  $\alpha_{RP}$  (L/mg) are the isotherm constants and  $\beta_{RP}$  is an exponent with values between 0 and 1. According to the statistical parameters ( $R^2$ , MAPE, and  $\chi^2$ ), RP was the model that best fit the experimental data; Fig. 4b and c shows the predicted (dashed line) and experimental (dots) values.

The  $K_{RP}$  parameter decreased with increasing temperature at both pHs (Table 5), indicating that PVA-Ch sorbent films heat-crosslinked at 160°C-1 h, presented a higher adsorption capacity at lower temperatures [73]; the  $\alpha_{RP}$  parameter followed the same trend. Similar results were published by Dotto et al. [73] for the adsorption of Acid Red 18 azo dye onto chitosan films. These findings are in agreement with the results reported by Pérez-Calderón et al. [68] using chitosan hydrogels cross-linked with oxalic acid for the removal of Reactive Red 195 dye.

### 3.7. Dye-sorbent interaction

The TGA thermograms corresponding to the heat-crosslinked film before and after the adsorption process were acquired

**Table 5**

Equations and parameters of adsorption isotherm models tested for the removal of Acid Orange 7 at different temperatures and pH using PVA-Ch sorbent films crosslinked at 160°C-1h.

Model		pH Conditions	
		pH = 2.5	pH = 4.0
Langmuir $Q_e = \frac{Q_m K_L C_e}{1 + K_L C_e}$ (15)	$Q_m$	678.0	100.7
	$K_L$	0.27	0.06
	$\chi^2$	36.7	0.22
	$R^2$	0.90	0.99
	MAPE	3.25	0.02
Freundlich $Q_e = K_F C_e^{1/n}$ (16)	$K_F$	279.7	34.9
	$n$	6.22	5.71
	$\chi^2$	17.8	50.2
	$R^2$	0.95	0.86
	MAPE	2.57	1.66
Dubinin – Radushkevich $Q_e = Q_{DR} \exp^{-\epsilon^2 B_{DR}}$ (17)	$Q_{DR}$	528.9	91.1
	$B_{DR}$	0.51	28.7
	$E \times 10^{-2}$	9.9	1.3
	$\chi^2$	536.6	47.9
	$R^2$	0.74	0.87
	MAPE	5.13	50.1
$\epsilon = R.T.Ln\left(1 + \frac{1}{C_e}\right)$ (17-1) $E = 1/(2.B_{DR})^{0.5}$ (17-2)	$K_{RP}$	455.5	5.82
	$\alpha_{RP}$	5.19	0.05
	$\beta$	0.89	0.99
	$\chi^2$	255.2	0.25
	$R^2$	0.99	0.99
	MAPE	0.02	0.03

Units of the parameters used in the models.

 $C_e$ : Equilibrium Concentration [mg/L]  $Q_m$ : Maximum adsorption capacity [mg/g]  $K_L$ : Constant Langmuir model  $K_F$ : Adsorption capacity coefficient [(mg/g)(mg.L)-1/n]  $n$ : Adsorption intensity  $\alpha_{RP}$ : Coefficient of Redlich-Peterson mode [L/mg]  $K_{RP}$ : Coefficient of Redlich-Peterson model. $\beta_{RP}$ : Exponent of Redlich-Peterson model  $Q_{DR}$ : Maximum adsorp. Capacity [mg/g]. $\epsilon$ : Polanyi potential [kJ/mol]  $B_{DR}$ : Constant related to the adsorption energy [mol/kj<sup>2</sup>]. $E$  average free adsorption energy [E, kJ/mol].

(Fig. 5a and b). The first stage corresponded to the dehydration of the materials with temperatures close to 100°C. The second thermal stage for the material before adsorption corresponded to polymeric degradation (result discussed in section 3.3). DTG curves of films with AO7 exhibited shifts of the maximum temperatures to higher values in the first and second stages due to the additional degradation of dye compounds while the maximum of the third stage practically disappeared. In this latter case, the residual weight was much higher than for films without adsorption of AO7 due to the presence of the dye interacting in the system (Fig. 5b, Table 3).

The interactions between the dye and the thermally crosslinked PVA-Ch films were studied by using ATR-FTIR. The ATR-FTIR spectra of the PVA-Ch sorbent films thermally crosslinked (160°C-1h), before and after adsorption at different pH conditions (4.0 and 2.5) as well as of the AO7 dye, are shown in Fig. 5c.

The characteristic signals of the PVA-Ch film heat-treated at 160°C-1h are described in section 3.2. The AO7 dye spectrum showed bands at 3673 and 3084 cm<sup>-1</sup> attributed to the stretching -NH, -OH groups, and the resonant aromatic structure = CH. The peaks at 2925 and 2854 cm<sup>-1</sup> were assigned to asymmetric and symmetric stretching of aliphatic CH. Other bands located at 1627 cm<sup>-1</sup> (aromatic ring vibrations) [78], 1598 cm<sup>-1</sup> stretching of the C=N, 1556 cm<sup>-1</sup> due to stretching of azo group N=N [79], 1506 and 1394 cm<sup>-1</sup> (vibrational stretching of the C-N bond), 1453 cm<sup>-1</sup> symmetric stretching of the -N-C=N, 1318 cm<sup>-1</sup> (SO<sub>2</sub> S=O group vibrations), 1180 cm<sup>-1</sup> (phenolic -C-OH group vibrations), 1032 cm<sup>-1</sup> (-C-OH and/or -CN stretching, and 697 cm<sup>-1</sup> (-S=O stretching) [80] were also observed.

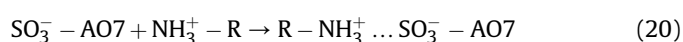
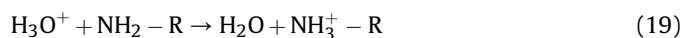
The modifications in the film spectra before the adsorption process (160°C-1h) and after at different adsorption conditions (pH = 2.5 and 4.0) were due to the interaction of the protonated amino groups (-NH<sub>3</sub><sup>+</sup>) of the chitosan and the sulfonate group (R-SO<sub>3</sub><sup>-</sup>) of the dye. The bands located at wavelengths ranging

between 3700 and 3000 cm<sup>-1</sup> underwent changes due to intermolecular forces, such as hydrogen bonds.

In the case of dye adsorption at pH 2.5 (Fig. 5c), the film spectrum showed the presence of two signals at 3487 and 3370 cm<sup>-1</sup> characteristics of AO7 dye. Also, the intensity of the shoulder at 2885 cm<sup>-1</sup> decreased due to the -NH<sub>3</sub><sup>+</sup>-SO<sub>3</sub><sup>-</sup> interaction [81]. The appearance of a small band at 1486 cm<sup>-1</sup> due to C-N vibrational stretching was observed indicating a displacement of this radical of the dye originally located at 1506 cm<sup>-1</sup>; this confirmed that hydrogen bonds and/or electrostatic interactions were involved in the adsorption process [78].

When the adsorption process was carried out at pH 4.0, the band at 2885 cm<sup>-1</sup> was also observed. The signal located at 1085 cm<sup>-1</sup> was modified and amplified after the adsorption process and the presence of a signal at 1029 cm<sup>-1</sup> was observed; these two signals correspond to the vibrations of the stretching of the C-OH alcoholic group characteristic of polysaccharides such as chitosan [82].

The reported results showed that pH played an essential role during the adsorption process. The optimum pH for adsorption was 2.5. Under these acidic conditions most of the amino groups of chitosan were protonated (Eq. 19), and electrostatic interactions were generated with the sulfonate groups (-SO<sub>3</sub><sup>-</sup>) of the dye [83] (Eq. 20). The proposed interaction mechanism is:



### 3.8. Effect of competitive ions

The presence of ions affects the adsorption process, hence the competitive effect of these ions on the removal of the synthetic dye

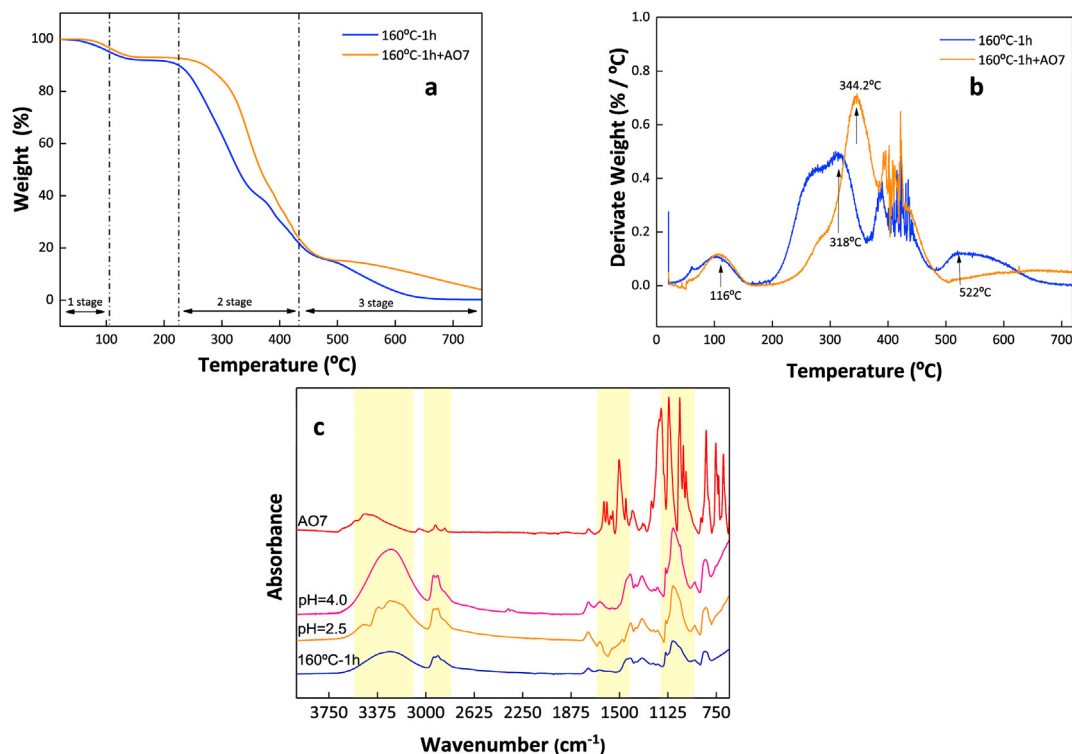


Fig. 5. Thermal behavior of the PVA-Ch sorbent film thermally cross-linked at 160°C-1h before and after the adsorption process of Acid Orange 7 dye (160°C-1h + AO7): a) TGA and b) first DTG derivative. c) ATR-FTIR spectra of AO7 dye, sorbent film (160°C-1h), and sorbent film under different adsorption pH (pH = 2.5 and 4.0).

AO7 was studied (Fig. 6). At pH 2.5, in the presence of Cl<sup>-</sup> ion, the adsorption capacity (Q) was reduced by 21.2% and the percentage of removal (Re%) was 8.2% in comparison to the control system (without the presence of competitive ions); however, the HCO<sub>3</sub><sup>-</sup> ion generated a reduction by 59.3% for Q and 56.6% for Re%. These results showed that the presence of highly electronegative species (SO<sub>4</sub><sup>2-</sup> and HCO<sub>3</sub><sup>-</sup>) affected the removal process at pH 2.5 (maximum removal) due to the competition between the sulfonate groups of the dye and the ions in solution by the vacant active sites (protonated amino groups) of the sorbent material [84].

Even in systems with the four ions present, the removal process was not significantly affected at pH 4.0. In all cases, the electrical conductivity was determined at the beginning of the test (t = 0) and

at the end (t = 24 h). The results (Table 6) indicated that there was a decline in the electrical conductivity at the end of the test, thus the systems showed a decrease of the ions in solution due to their interaction with the sorbent material.

### 3.9. Regeneration and reutilization of material

According to Chatterjee et al. [85] and Guibal [86], the sorbent materials with the presence of chitosan can be efficiently regenerated using methodologies such as changes in the pH of the medium to alkaline conditions. Five continuous cycles of adsorption at pH = 2.5 and desorption at pH = 12 were performed; the adsorption capacity (Q) and physical characterization parameters such as

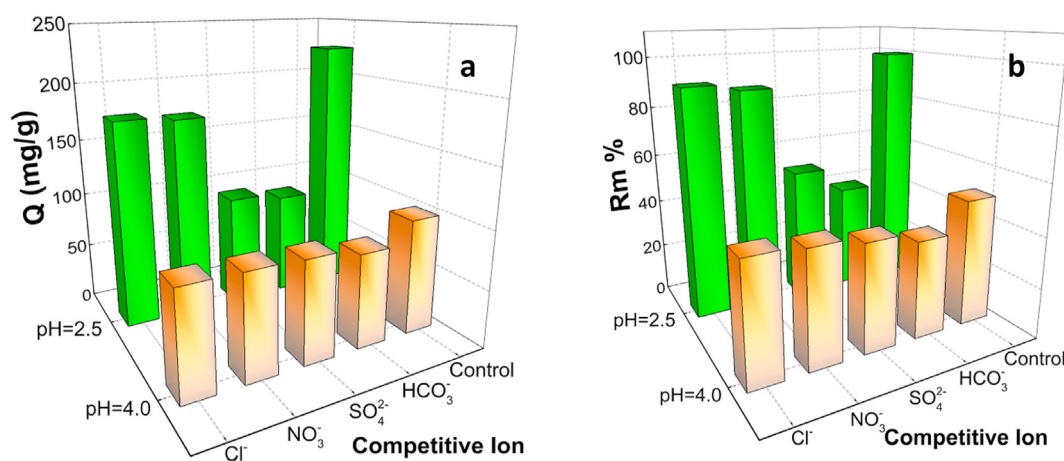


Fig. 6. Effect of competitive ions on the: a. adsorption capacity (Q) and b. removal percentage (Re%) for dye AO7. Conditions: C<sub>i</sub> AO7 = 170 mg/L; C<sub>i</sub> Ion = 25 mg/L; T = 298 K; 150 rev/min.

**Table 6**

Variation of electrical conductivity (ms/cm) between initial time (t = 0) and final time (t = 24 h) for the different competitive ions tested. Standard deviation is shown in parentheses; n = 3.

pH	Cl <sup>-</sup>		NO <sub>3</sub> <sup>-</sup>		SO <sub>4</sub> <sup>2-</sup>		HCO <sub>3</sub> <sup>-</sup>	
	t = 0 h	t = 24 h	t = 0 h	t = 24 h	t = 0	t = 24 h	t = 0	t = 24 h
2.5	4.07 (0.02)	3.74 (0.01)	3.93 (0.04)	3.74 (0.11)	5.92 (0.4)	5.59 (0.4)	6.22 (0.08)	6.20 (0.1)
4.0	3.41 (0.08)	3.17 (0.07)	3.24 (0.03)	3.18 (0.09)	4.92 (0.5)	4.93 (0.3)	5.78 (0.07)	5.71 (0.5)

browning index (BI), contact angle (CA), and mechanical properties (tensile stress (E) and elongation% (ε<sub>r</sub>%)), were analyzed for the PVA-Ch cross-linked sorbent films at different stages of the regeneration and reutilization process. The considered stages were: before the first adsorption cycle (BFA), after the first adsorption cycle (AFA), after the last adsorption cycle (ALA), and finally after the last desorption cycle (ALD); the results are shown in Fig. 7-a.

The results obtained from ALD were compared with those found for AFA. The Re% and Q were only reduced by 14.2% and 15.3%,

respectively. These results indicated that the material was not affected by the constant adsorption/desorption cycles keeping the excellent removal properties of the AO7 dye.

Concerning the physical properties evaluated and comparing the results before the first adsorption cycle (BFA) with ALD, it can be inferred that the mechanical properties were not degraded. The ALD films presented higher ε<sub>r</sub>%, percent elongation (p < 0.05) compared to the BFA films. On the other hand, E did not present significant differences (p > 0.05) showing that the desorption

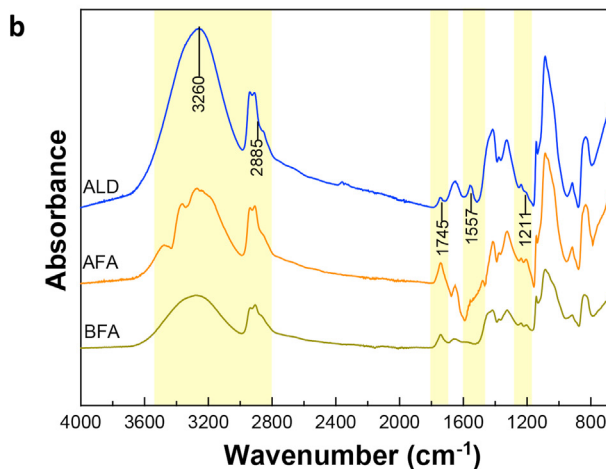
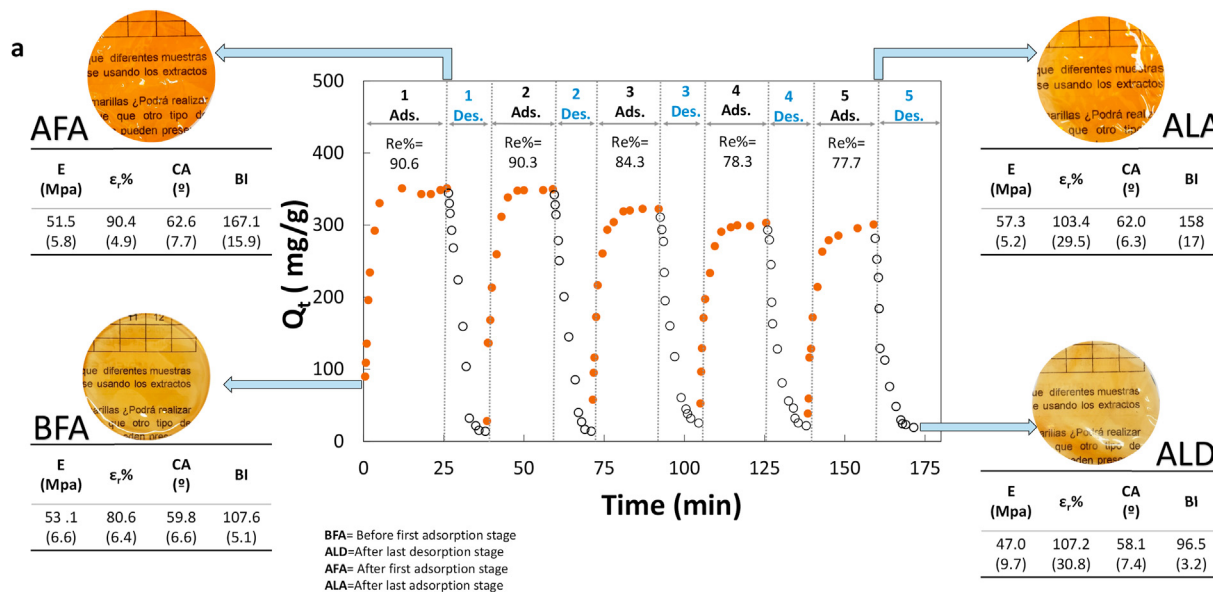


**Fig. 7. a.** Adsorption-desorption cycles and physical characteristics of adsorbent films at different stages of the process: before the first adsorption cycle (BFA), after the first adsorption cycle (AFA), after the last adsorption cycle (ALA), and after the last desorption cycle (ALD). Adsorption conditions: pH = 2.5; C<sub>i</sub> = 300 mg/L; 150 rev/min; T = 293 K. Desorption conditions: pH = 12.5 (NaOH 1 M); 150 rev/min; T = 293 K. **b.** ATR-FTIR spectra of heat cross-linked PVA-Ch films BFA, AFA, and ALD.

process did not alter the molecular interactions achieved by the physical cross-linking treatment (data shown in the Tables inserted in Fig. 7-a).

The structural changes of the material at the end of the fifth desorption cycle (ALD) were analyzed by ATR-FTIR spectra (Fig. 7-b). ALD film spectrum showed a signal at  $3260\text{ cm}^{-1}$  similar to the spectrum of the film before the first removal process (cross-linked film at  $160^\circ\text{C}$ -1h without dye) proving that a considerable amount of the dye molecules were released in the regeneration of the material.

Considering the ALD regenerated films and AFA films at pH 2.5, the signal at  $2885\text{ cm}^{-1}$  did not change, indicating that although dye was released from the material produced by the regeneration process, the  $-\text{NH}_3^+ - \text{SO}_3^{1-}$  interaction was maintained in the matrix [81].

In the regeneration process, the alkaline pH conditions led to the release of dye molecules which interacted electrostatically with the adsorbent film. This phenomenon was produced by the deprotonation of the amine groups of the chitosan generating free amino groups [87] that was corroborated by the appearance of the peak at  $1557\text{ cm}^{-1}$  characteristic of the amide II group in ALD film.

#### 4. Conclusions

A hybrid adsorbent film based on PVA and Ch was developed for the removal of the azo dye Acid Orange 7 (AO7) used in the textile industry and present in contaminated industrial wastewater. To improve the physical stability in aqueous media, the material was submitted to a curing process with different time-temperature combinations. The best condition to achieve high removal capacity without weight loss was the combination of  $160^\circ\text{C}$ -1h. Characterization studies showed that the polymeric network was physically cross-linked after the thermal curing process. This physical crosslinking process was effective to diminish the weight loss, reaching an average value of 0.007% at pH = 2.5. This characteristic is essential in the development of sorbent materials from biodegradable polymers.

The material showed chemical and physical stability at highly acidic conditions due to the crosslinking of the polymeric network.

From the adsorption tests of the azo dye AO7, a high removal efficiency (>90%) was achieved at pH = 2.5. Results were used to model the corresponding adsorption kinetics and isotherms; the Ps.1 order kinetic model and the Redlich-Peterson isotherm gave the best fit. Using the Langmuir model, it was possible to calculate the maximum adsorption capacity ( $Q_m$ ) which was as far as the authors know, the highest value reported in literature.

ATR-FTIR allowed the setting of the interactions between PVA and chitosan, as well as among the polymers and the dye. At pH = 2.5 there were electrostatic interactions and hydrogen bonds between the PVA-Ch sorbent films and the molecules of the dye.

The analysis of the adsorption/regeneration/reutilization allowed determining that after five cycles, the adsorption capacity for the removal of the AO7 dye was maintained.

The physical curing treatment avoided the use of chemical crosslinking agents, generating biosorbent matrices that would have a low environmental impact related to the generation of polluting by-products.

Thus, the use of the developed eco-compatible biodegradable materials would allow easy regeneration without losing removal selectivity, a key feature in the development of environmentally friendly sorbent materials.

#### Author's contributions

JPC: Methodology, investigation, writing-review. DAMS: Methodology, investigation. NZ: Formal analysis, writing-review &

editing. A.P.: Writing-original draft, formal analysis, writing-review & editing, funding acquisition.

All authors have approved the final version of the manuscript.

#### Declaration of competing interest

The authors declared no potential conflicts of interest with respect to the research, authorship, and/or publication of this article.

#### Acknowledgments

This work was supported by the Argentinean Agency for the Scientific and Technological Promotion (ANPCyT) (Project PICT 2019-02008 and PICT 2017-0831).

#### References

- [1] M. McFall-Johnsen, These Facts Show How Unsustainable the Fashion Industry Is, World Economic Forum, 2020. <https://bit.ly/3kblCsK>. (Accessed 26 April 2022).
- [2] M. Ağtaş, Ö. Yılmaz, M. Dilaver, K. Alp, İ. Koyuncu, Hot water recovery and reuse in textile sector with pilot scale ceramic ultrafiltration/nanofiltration membrane system, *J. Clean. Prod.* 256 (2020) 120359, <https://doi.org/10.1016/j.jclepro.2020.120359>.
- [3] J. Mittal, Recent progress in the synthesis of Layered Double Hydroxides and their application for the adsorptive removal of dyes: a review, *J. Environ. Manag.* 295 (2021) 113017, <https://doi.org/10.1016/j.jenvman.2021.113017>.
- [4] H. Pan, J. Feng, G.-X. He, C.E. Cerniglia, H. Chen, Evaluation of impact of exposure of Sudan azo dyes and their metabolites on human intestinal bacteria, *Anaerobe* 18 (2012) 445–453, <https://doi.org/10.1016/j.anaerobe.2012.05.002>.
- [5] A. Patel, S. Soni, J. Mittal, A. Mittal, C. Arora, Sequestration of crystal violet from aqueous solution using ash of black turmeric rhizome, *Desalination Water Treat.* 220 (2021) 342–352, <https://doi.org/10.5004/dwt.2021.26911>.
- [6] A. Mariyam, J. Mittal, F. Sakina, R.T. Baker, A.K. Sharma, A. Mittal, Efficient batch and Fixed-Bed sequestration of a basic dye using a novel variant of ordered mesoporous carbon as adsorbent, *Arab. J. Chem.* 14 (2021) 103186, <https://doi.org/10.1016/j.arabjc.2021.103186>.
- [7] J. Mittal, A. Mariyam, F. Sakina, R.T. Baker, A.K. Sharma, A. Mittal, Batch and bulk adsorptive removal of anionic dye using metal/halide-free ordered mesoporous carbon as adsorbent, *J. Clean. Prod.* 321 (2021) 129060, <https://doi.org/10.1016/j.jclepro.2021.129060>.
- [8] M. Yusuf, M.A. Khan, M. Otero, E.C. Abdullah, M. Hosomi, A. Terada, S. Riya, Synthesis of CTAB intercalated graphene and its application for the adsorption of AR265 and AO7 dyes from water, *J. Colloid Interface Sci.* 493 (2017) 51–61, <https://doi.org/10.1016/j.jcis.2017.01.015>.
- [9] V.M. Bishop, A.A.P. Mansur, E.F. Barbosa-Stancioli, H.S. Mansur, Biocompatibility of nanostructured chitosan/poly(vinyl alcohol) blends chemically crosslinked with genipin for biomedical applications, *J. Biomed. Nanotechnol.* 6 (2010) 166–175, <https://doi.org/10.1166/jbn.2010.1110>.
- [10] V.K. Gupta, A. Mittal, V. Gajbe, J. Mittal, Removal and recovery of the hazardous azo dye acid orange 7 through adsorption over waste materials: bottom ash and de-oiled soya, *Ind. Eng. Chem. Res.* 45 (2006) 1446–1453, <https://doi.org/10.1021/ie051111f>.
- [11] K. Vinodgopal, D.E. Wynkoop, P. V. Kamat, Environmental photochemistry on semiconductor surfaces: photosensitized degradation of a textile azo dye, acid orange 7, on TiO<sub>2</sub> particles using visible light, *Environ. Sci. Technol.* 30 (1996) 1660–1666, <https://doi.org/10.1021/es950655d>.
- [12] X. Pan, M. Zhang, H. Liu, S. Ouyang, N. Ding, P. Zhang, Adsorption behavior and mechanism of acid orange 7 and methylene blue on self-assembled three-dimensional MgAl layered double hydroxide: experimental and DFT investigation, *Appl. Surf. Sci.* 522 (2020) 146370, <https://doi.org/10.1016/j.apsusc.2020.146370>.
- [13] K.W. Jung, B.H. Choi, M.J. Hwang, T.U. Jeong, K.H. Ahn, Fabrication of granular activated carbons derived from spent coffee grounds by entrapment in calcium alginate beads for adsorption of acid orange 7 and methylene blue, *Bioresour. Technol.* 219 (2016) 185–195, <https://doi.org/10.1016/j.biortech.2016.07.098>.
- [14] G. Crini, G. Torri, E. Lichtfouse, G.Z. Kyzas, L.D. Wilson, N. Morin-crini, Cross-linked chitosan-based hydrogels for dye removal, in: G. Crini, E. Lichtfouse (Eds.), *Sustain. Agric. Rev.* 36, Springer, Cham, 2019, pp. 381–425, <https://doi.org/10.1007/978-3-030-16581-9>.
- [15] J. Mittal, R. Ahmad, A. Mariyam, V.K. Gupta, A. Mittal, Expedient and enhanced sequestration of heavy metal ions from aqueous environment by papaya peel carbon: a green and low-cost adsorbent, *Desalination Water Treat.* 210 (2021) 365–376, <https://doi.org/10.5004/dwt.2021.26562>.

- [16] G. Crini, Non-conventional low-cost adsorbents for dye removal: a review, *Bioresour. Technol.* 97 (2006) 1061–1085, <https://doi.org/10.1016/j.biortech.2005.05.001>.
- [17] V.K. Gupta, Suhas, Application of low-cost adsorbents for dye removal - a review, *J. Environ. Manag.* 90 (2009) 2313–2342, <https://doi.org/10.1016/j.jenvman.2008.11.017>.
- [18] F. Peng, P.-W. He, Y. Luo, X. Lu, Y. Liang, J. Fu, Adsorption of phosphate by biomass char deriving from fast pyrolysis of biomass waste, *CLEAN – soil, Air, Water* 40 (2012) 493–498, <https://doi.org/10.1002/clean.201100469>.
- [19] E. Haque, J.W. Jun, S.H. Jhung, Adsorptive removal of methyl orange and methylene blue from aqueous solution with a metal-organic framework material, iron terephthalate (MOF-235), *J. Hazard Mater.* 185 (2011) 507–511, <https://doi.org/10.1016/j.jhazmat.2010.09.035>.
- [20] R. Dhodapkar, N.N. Rao, S.P. Pande, S.N. Kaul, Removal of basic dyes from aqueous medium using a novel polymer: Jalshakti, *Bioresour. Technol.* 97 (2006) 877–885, <https://doi.org/10.1016/j.biortech.2005.04.033>.
- [21] I. Humelnicu, A. Băiceanu, M.-E. Ignat, V. Dulman, The removal of Basic Blue 41 textile dye from aqueous solution by adsorption onto natural zeolitic tuff: kinetics and thermodynamics, *Process Saf. Environ. Protect.* 105 (2017) 274–287, <https://doi.org/10.1016/j.psep.2016.11.016>.
- [22] A. Alhujaily, H. Yu, X. Zhang, F. Ma, Adsorptive removal of anionic dyes from aqueous solutions using spent mushroom waste, *Appl. Water Sci.* 10 (2020) 183, <https://doi.org/10.1007/s13201-020-01268-2>.
- [23] J.B. Dima, C. Sequeiros, N.E. Zaritzky, Hexavalent chromium removal in contaminated water using reticulated chitosan micro/nanoparticles from seafood processing wastes, *Chemosphere* 141 (2015) 100–111.
- [24] N. Morin-crini, E. Lichtfouse, G. Torri, G. Crini, Fundamentals and applications of chitosan, in: G. Crini, E. Lichtfouse (Eds.), *Sustain. Agric. Rev.* 35, Springer, Cham, 2019, pp. 49–123, <https://doi.org/10.1007/978-3-030-16538-3>.
- [25] R.E.K. Billah, M.A. Khan, S.M. Wabaidur, B.H. Jeon, A.M. Amira, H. Majdoubi, Y. Haddaji, M. Agunaou, A. Soufiane, Chitosan/phosphate rock-derived natural polymeric composite to sequester divalent copper ions from water, *Nanomaterials* 11 (2021) 1–17, <https://doi.org/10.3390/nano11082028>.
- [26] A.H. Mijinyawa, G. Durga, A. Mishra, Preparation and application of chitosan-based membrane: focusing on dye removal, in: S. Muthu, A. Khadir (Eds.), *Membr. Based Methods Dye Contain. Wastewater. Sustainable Text. Prod. Process. Manuf. Chem.*, Springer, Singapore, 2022, pp. 121–179, [https://doi.org/10.1007/978-981-16-4823-6\\_6](https://doi.org/10.1007/978-981-16-4823-6_6).
- [27] P. Sirajudheen, N.C. Poovathumkuzhi, S. Vigneshwaran, B.M. Chelaveetil, S. Meenakshi, Applications of chitin and chitosan based biomaterials for the adsorptive removal of textile dyes from water — a comprehensive review, *Carbohydr. Polym.* 273 (2021) 118604, <https://doi.org/10.1016/j.carbpol.2021.118604>.
- [28] X. Liu, L. Zhang, Removal of phosphate anions using the modified chitosan beads: adsorption kinetic, isotherm and mechanism studies, *Powder Technol.* 277 (2015) 112–119, <https://doi.org/10.1016/j.powtec.2015.02.055>.
- [29] L. Huang, Z. Luo, X. Huang, Y. Wang, J. Yan, W. Liu, Y. Guo, S.R. Babu Arulmani, M. Shao, H. Zhang, Applications of biomass-based materials to remove fluoride from wastewater: a review, *Chemosphere* (2022) 134679, <https://doi.org/10.1016/j.chemosphere.2022.134679>.
- [30] H. Karimi-Maleh, A. Ayati, R. Davoodi, B. Tanhaei, F. Karimi, S. Malekmohammadi, Y. Orooji, L. Fu, M. Sillanpää, Recent advances in using of chitosan-based adsorbents for removal of pharmaceutical contaminants: a review, *J. Clean. Prod.* 291 (2021) 125880, <https://doi.org/10.1016/j.jclepro.2021.125880>.
- [31] E. Chiellini, A. Corti, S. D'Antone, R. Solaro, Biodegradation of poly (vinyl alcohol) based materials, *Prog. Polym. Sci.* 28 (2003) 963–1014, [https://doi.org/10.1016/S0079-6700\(02\)00149-1](https://doi.org/10.1016/S0079-6700(02)00149-1).
- [32] A. Woźniak, M. Biernat, Methods for crosslinking and stabilization of chitosan structures for potential medical applications, *J. Bioact. Compat. Polym.* (2022) 1–17, <https://doi.org/10.1177/08839115221085738>.
- [33] L. Casey, L. Wilson, Investigation of chitosan-PVA composite films and their adsorption properties, *J. Geosci. Environ. Protect.* 3 (2015) 78–84, <https://doi.org/10.4236/gep.2015.32013>.
- [34] W.S. Wan Ngah, L.C. Teong, M.A.K.M. Hanafiah, Adsorption of dyes and heavy metal ions by chitosan composites: a review, *Carbohydr. Polym.* 83 (2011) 1446–1456, <https://doi.org/10.1016/j.carbpol.2010.11.004>.
- [35] Z. Wang, Y. Li, X. Xie, Z. Wang, Bifunctional MnFe2O4/chitosan modified biochar composite for enhanced methyl orange removal based on adsorption and photo-Fenton process, *Colloid. Surf. Physicochem. Eng. Asp.* 613 (2021) 126104, <https://doi.org/10.1016/j.colsurfa.2020.126104>.
- [36] N.H. Elsayed, R.A.S. Alatawi, M. Monier, Amidoxime modified chitosan based ion-imprinted polymer for selective removal of uranyl ions, *Carbohydr. Polym.* 256 (2021) 117509, <https://doi.org/10.1016/j.carbpol.2020.117509>.
- [37] R.E.K. Billah, M.A. Khan, Y.K. Park, A. Am, H. Majdoubi, Y. Haddaji, B.H. Jeon, A comparative study on hexavalent chromium adsorption onto chitosan and chitosan-based composites, *Polymers (Basel)* 13 (2021) 1–15, <https://doi.org/10.3390/polym13193427>.
- [38] A. Rajeswari, A. Amalraj, A. Pius, Adsorption studies for the removal of nitrate using chitosan/PEG and chitosan/PVA polymer composites, *J. Water Proc. Eng.* 9 (2016) 123–134, <https://doi.org/10.1016/j.jwpe.2015.12.002>.
- [39] M. Azmana, S. Mahmood, A.R. Hilles, A. Rahman, M.A. Bin Arifin, S. Ahmed, A review on chitosan and chitosan-based bionanocomposites: promising material for combatting global issues and its applications, *Int. J. Biol. Macromol.* 185 (2021) 832–848, <https://doi.org/10.1016/j.ijbiomac.2021.07.023>.
- [40] X. Li, Y. Li, S. Zhang, Z. Ye, Preparation and characterization of new foam adsorbents of poly(vinyl alcohol)/chitosan composites and their removal for dye and heavy metal from aqueous solution, *Chem. Eng. J.* 183 (2012) 88–97, <https://doi.org/10.1016/j.cej.2011.12.025>.
- [41] N.M. Mahmoodi, Z. Mokhtari-Shourijeh, Preparation of PVA-chitosan blend nanofiber and its dye removal ability from colored wastewater, *Fibers Polym.* 16 (2015) 1861–1869, <https://doi.org/10.1007/s12221-015-5371-1>.
- [42] W. Wang, H. Zhang, J. Shen, M. Ye, Facile preparation of magnetic chitosan/poly (vinyl alcohol) hydrogel beads with excellent adsorption ability via freezing-thawing method, *Colloid. Surf. Physicochem. Eng. Asp.* 553 (2018) 672–680, <https://doi.org/10.1016/j.colsurfa.2018.05.094>.
- [43] H.-W. Leung, Ecotoxicology of glutaraldehyde: review of environmental fate and effects studies, *Ecotoxicol. Environ. Saf.* 49 (2001) 26–39, <https://doi.org/10.1006/eesa.2000.2031>.
- [44] B. Bolto, T. Tran, M. Hoang, Z. Xie, Progress in Polymer Science Crosslinked poly (vinyl alcohol) membranes, *Prog. Polym. Sci.* 34 (2009) 969–981, <https://doi.org/10.1016/j.progpolymsci.2009.05.003>.
- [45] P. Guerrero, I. Zugasti, A. Etxabide, H.N. Bao, T. Trang Si, M. Peñalba, K. de la Caba, Effect of fructose and ascorbic acid on the performance of cross-linked fish gelatin films, *Polymer* 12 (2020), <https://doi.org/10.3390/polym12030570>.
- [46] V. Belessi, G. Romanos, N. Boukos, D. Lambropoulou, C. Tralalis, Removal of Reactive Red 195 from aqueous solutions by adsorption on the surface of TiO<sub>2</sub> nanoparticles, *J. Hazard Mater.* 170 (2009) 836–844, <https://doi.org/10.1016/j.jhazmat.2009.05.045>.
- [47] J. Pérez-Calderón, M. V Santos, N. Zaritzky, Reactive Red 195 dye removal using chitosan coacervated particles as bio-sorbent: analysis of kinetics, equilibrium and adsorption mechanisms, *J. Environ. Chem. Eng.* 6 (2018) 6749–6760, <https://doi.org/10.1016/j.jece.2018.10.039>.
- [48] D. Aycan, N.A. Yayla, Y.A. Ayden, Chitosan polyvinyl alcohol blend films for ibuprofen encapsulation: fabrication, characterization and kinetics, *Polym. Degrad. Stabil.* 181 (2020) 109346, <https://doi.org/10.1016/j.polydegradstab.2020.109346>.
- [49] A. Çay, M. Miraftab, E. Perrin Akçakoca Kumbasar, Characterization and swelling performance of physically stabilized electrospun poly(vinyl alcohol)/chitosan nanofibres, *Eur. Polym. J.* 61 (2014) 253–262, <https://doi.org/10.1016/j.eurpolymj.2014.10.017>.
- [50] Y.U. Xianda, W. Anlai, Water-vapor permeability of polyvinyl alcohol films, *Desalination* 62 (1987) 293–297, [https://doi.org/10.1016/0011-9164\(87\)87030-3](https://doi.org/10.1016/0011-9164(87)87030-3).
- [51] T. Koyano, N. Koshizaki, H. Umehara, M. Nagura, N. Minoura, Surface states of PVA/chitosan blended hydrogels, *Polymer (Guildf.)* 41 (2000) 4461–4465, [https://doi.org/10.1016/S0032-3861\(99\)00675-8](https://doi.org/10.1016/S0032-3861(99)00675-8).
- [52] C.-H. Chen, F.-Y. Wang, C.-F. Mao, C.-H. Yang, Studies of chitosan. I. Preparation and characterization of chitosan/poly(vinyl alcohol) blend films, *J. Appl. Polym. Sci.* 105 (2007) 1086–1092, <https://doi.org/10.1002/app.26257>.
- [53] E.A. El-Hefian, M.M. Nasef, A.H. Yahaya, Preparation and characterization of chitosan/poly(vinyl alcohol) blended films: mechanical, thermal and surface investigations, *E-J. Chem.* 8 (2011) 969062, <https://doi.org/10.1155/2011/969062>.
- [54] S. Bahrami, S. Kordestani, H. Mirzadeh, P. Mansouri, Poly (vinyl alcohol)-chitosan blends: preparation, mechanical and physical properties, *Iran, Polym. J.* 12 (2003) 139–146, <https://www.sid.ir/en/Journal/ViewPaper.aspx?ID=12706>.
- [55] J.H. Kim, J.Y. Kim, Y.M. Lee, K.Y. Kim, Properties and swelling characteristics of cross-linked poly(vinyl alcohol)/chitosan blend membrane, *J. Appl. Polym. Sci.* 45 (1992) 1711–1717, <https://doi.org/10.1002/app.1992.070451004>.
- [56] U. Habiba, T.A. Siddique, S. Talebian, J.L. Lee, A. Salleh, B.C. Ang, A.M. Affi, Effect of deacetylation on property of electrospun Chitosan/PVA nanofibrous membrane and removal of Methyl orange, Fe (III) and Cr (VI) ions, *Carbohydr. Polym.* 177 (2017) 32–39, <https://doi.org/10.1016/j.carbpol.2017.08.115>.
- [57] K. Hedayatyanfard, S. Bagheri-Khouljenani, A. Hashemi, S.A. Ziai, Semi-IPN films and electrospun nanofibers based on chitosan/PVA as an antibacterial wound dressing, *Iran, J. Pharm. Res.* 18 (2019) 1156–1167, <https://doi.org/10.22037/ijpr.2019.1100712>.
- [58] U. Habiba, T.C. Joo, T.A. Siddique, A. Salleh, B.C. Ang, A.M. Affi, Effect of degree of deacetylation of chitosan on adsorption capacity and reusability of chitosan/polyvinyl alcohol/TiO<sub>2</sub> nano composite, *Int. J. Biol. Macromol.* (2017), <https://doi.org/10.1016/j.ijbiomac.2017.07.007>.
- [59] D. Nataraj, R. Reddy, N. Reddy, Crosslinking electrospun poly (vinyl alcohol) fibers with citric acid to impart aqueous stability for medical applications, *Eur. Polym. J.* 124 (2020) 109484, <https://doi.org/10.1016/j.eurpolymj.2020.109484>.
- [60] S. Rivero, M.A. García, A. Pinotti, Heat treatment to modify the structural and physical properties of chitosan-based films, *J. Agric. Food Chem.* 60 (2012) 492–499, <https://doi.org/10.1021/jf204077k>.
- [61] U. Habiba, A.M. Affi, A. Salleh, B.C. Ang, Chitosan/(polyvinyl alcohol)/zeolite electrospun composite nanofibrous membrane for adsorption of Cr<sup>6+</sup>, Fe<sup>3+</sup> and Ni<sup>2+</sup>, *J. Hazard Mater.* 322 (2017) 182–194, <https://doi.org/10.1016/j.jhazmat.2016.06.028>.
- [62] L. Zhang, G. Zhang, J. Lu, H. Liang, Preparation and characterization of carboxymethyl cellulose/polyvinyl alcohol blend film as a potential coating, *Mater. Polym. Plast. Technol. Eng.* 52 (2013) 163–167, <https://doi.org/10.1080/03602559.2012.734361>.
- [63] V. Sinha, S. Chakma, Advances in the preparation of hydrogel for wastewater treatment: a concise review, *J. Environ. Chem. Eng.* 7 (2019) 103295, <https://doi.org/10.1016/j.jece.2019.103295>.

- [64] E. Parparita, C.N. Cheaburu, C. Vasile, Morphological, thermal and rheological characterization of polyvinyl alcohol/chitosan blends, *Cellul. Chem. Technol.* 46 (2012) 571–581.
- [65] K. Lewandowska, Miscibility and thermal stability of poly(vinyl alcohol)/chitosan mixtures, *Thermochim. Acta* 493 (2009) 42–48, <https://doi.org/10.1016/j.tca.2009.04.003>.
- [66] V.K. Rana, A.K. Pandey, R.P. Singh, B. Kumar, S. Mishra, C.-S. Ha, Enhancement of thermal stability and phase relaxation behavior of chitosan dissolved in aqueous l-lactic acid: using 'silver nanoparticles' as nano filler, *Macromol. Res.* 18 (2010) 713–720, <https://doi.org/10.1007/s13233-010-0801-9>.
- [67] N.A.N. Nik Malek, A.S. Mat Sihat, N.M. Khalifa, A.A. Kamaru, N.S. Sani, Adsorption of Acid Orange 7 by cetylpyridinium bromide modified sugarcane bagasse, *J. Teknol.* 2 (2016) 97–103, <https://doi.org/10.11113/jt.v78.7276>.
- [68] J. Pérez-Calderón, V. Santos M, N. Zaritzky, Synthesis, characterization and application of cross-linked chitosan/oxalic acid hydrogels to improve azo dye (Reactive Red 195) adsorption, *React. Funct. Polym.* (2020) 104699, <https://doi.org/10.1016/j.reactfunctpolym.2020.104699>.
- [69] M. Sillanpää, A.H. Mahvi, D. Balarak, A.D. Khatibi, Adsorption of Acid orange 7 dyes from aqueous solution using Polypyrrole/nanosilica composite: experimental and modelling, *Int. J. Environ. Anal. Chem.* (2021) 1–18, <https://doi.org/10.1080/03067319.2020.1855338>.
- [70] B. Naraghi, F. Zabihi, M.R. Narooie, M. Saeidi, H. Biglari, S. Lecturer, S. Lecturer, S. Lecturer, T. Heydariyeh, S. Lecturer, Removal of Acid Orange 7 dye from aqueous solutions by adsorption onto Kenya tea pulps; granulated shape, *Electron. Physician* 9 (2017) 4312–4321, <https://doi.org/10.19082/4312>.
- [71] E. Khosla, S. Kaur, P.N. Dave, Mechanistic study of adsorption of acid orange-7 over aluminum oxide nanoparticles, *J. Eng.* 2013 (2013), <https://doi.org/10.1155/2013/593534>.
- [72] S. Akazdam, M. Chafi, W. Yassine, B. Gourich, Removal of Acid Orange 7 dye from aqueous solution using the exchange resin Amberlite FPA-98 as an efficient adsorbent: kinetics, isotherms, and thermodynamics study, *J. Mater. Environ. Sci.* 8 (2017) 2993–3012.
- [73] G.L. Dotto, J.M. Moura, T.R.S. Cadaval, L.A.A. Pinto, Application of chitosan films for the removal of food dyes from aqueous solutions by adsorption, *Chem. Eng. J.* 214 (2013) 8–16, <https://doi.org/10.1016/j.cej.2012.10.027>.
- [74] J. Wu, Z. Dong, X. Li, P. Li, J. Wei, M. Hu, L. Geng, X. Peng, Constructing acid-resistant chitosan/cellulose nanofibrils composite membrane for the adsorption of methylene blue, *J. Environ. Chem. Eng.* 10 (2022) 107754, <https://doi.org/10.1016/j.jece.2022.107754>.
- [75] H. Nourmoradi, A.R. Ghiasvand, Z. Noorimotlagh, Removal of methylene blue and acid orange 7 from aqueous solutions by activated carbon coated with zinc oxide (ZnO) nanoparticles: equilibrium, kinetic, and thermodynamic study, *Desalination Water Treat.* 55 (2015) 252–262, <https://doi.org/10.1080/19443994.2014.914449>.
- [76] G. Mckay, H.S. Blair, J.R. Gardner, Adsorption of dyes on chitin. I. Equilibrium studies, *J. Appl. Polym. Sci.* 27 (1982) 3043–3057, <https://doi.org/10.1002/app.1982.070270827>.
- [77] M. Dubinin, L. Radushkevich, The equation of the characteristic curve of activated charcoal, *Proc. Acad. Sci. Phys. Chem. Sect.* 55 (1947) 327–329, <https://doi.org/10.4236/ojs.2014.41001>.
- [78] W. Wang, G. Tian, D. Wang, Z. Zhang, Y. Kang, L. Zong, A. Wang, All-into-one strategy to synthesize mesoporous hybrid silicate microspheres from naturally rich red palygorskite clay as high-efficient adsorbents, *Nat. Sci. Rep.* 6 (2016), <https://doi.org/10.1038/srep39599>.
- [79] L. Çelik, A. Öztürk, M.I. Abdullah, Biodegradation of reactive red 195 azo dye by the bacterium *Rhodopseudomonas palustris* 51ATA, *Afr. J. Microbiol. Res.* 6 (2012) 120–126, <https://doi.org/10.5897/AJMR11.1059>.
- [80] G.S. Ghodake, A.A. Talke, J.P. Jadhav, S.P. Govindwar, Potential of Brassica juncea in order to treat textile-effluent- contaminated sites, *Int. J. Phytoremediation* 11 (2009) 297–312, <https://doi.org/10.1080/15226510802429518>.
- [81] K. Takayama, M. Hirata, Y. Machida, T. Masada, T. Sannan, T. Nagai, Effect of interpolymer complex formation on bioadhesive property and drug release phenomenon of compressed tablet consisting of chitosan and sodium hyaluronate, *Chem. Pharm. Bull. (Tokyo)* 38 (1990) 1993–1997, <https://doi.org/10.1248/cpb.38.1993>.
- [82] G.Z. Kyzas, D.N. Bikiaris, N.K. Lazaridis, Low-swelling chitosan derivatives as biosorbents for basic dyes, *Langmuir* 24 (2008) 4791–4799, <https://doi.org/10.1021/la7039064>.
- [83] K.B. Tan, M. Vakili, B.A. Horri, P.E. Poh, A.Z. Abdullah, B. Salamatinia, Adsorption of dyes by nanomaterials: recent developments and adsorption mechanisms, *Separ. Purif. Technol.* 150 (2015) 229–242, <https://doi.org/10.1016/j.seppur.2015.07.009>.
- [84] Z. Zhu, M. Zhang, F. Liu, C. Shuang, C. Zhu, Y. Zhang, A. Li, Effect of polymeric matrix on the adsorption of reactive dye by anion-exchange resins, *J. Taiwan Inst. Chem. Eng.* 62 (2016) 98–103, <https://doi.org/10.1016/j.jtice.2016.01.017>.
- [85] S. Chatterjee, S. Chatterjee, B.P. Chatterjee, A.R. Das, A.K. Guha, Adsorption of a model anionic dye, eosin Y, from aqueous solution by chitosan hydrobeads, *J. Colloid Interface Sci.* 288 (2005) 30–35, <https://doi.org/10.1016/j.jcis.2005.02.055>.
- [86] E. Guibal, Interactions of metal ions with chitosan-based sorbents: a review, *Separ. Purif. Technol.* 38 (2004) 43–74, <https://doi.org/10.1016/j.seppur.2003.10.004>.
- [87] C.Y. Chen, J.C. Chang, A.H. Chen, Competitive biosorption of azo dyes from aqueous solution on the templated crosslinked-chitosan nanoparticles, *J. Hazard Mater.* 185 (2011) 430–441, <https://doi.org/10.1016/j.jhazmat.2010.09.051>.